Journal of Computational Physics 243 (2013) 323–343

Contents lists available at SciVerse ScienceDirect

Journal of Computational Physics

journal homepage: www.elsevier.com/locate/jcp

Exact PDF equations and closure approximations for advective-reactive transport

D. Venturi [a], D.M. Tartakovsky [b], A.M. Tartakovsky [c], G.E. Karniadakis [a,*]

[a] Division of Applied Mathematics, Brown University, Providence, RI 02912, USA
[b] Department of Mechanical and Aerospace Engineering, University of California, San Diego, La Jolla, CA 92093, USA
[c] Pacific Northwest National Laboratory, Richland, WA 99352, USA

ARTICLE INFO

Article history:
Received 28 March 2012
Accepted 5 March 2013
Available online 15 March 2013

Keywords:
PDF methods
Uncertainty quantification
Heterogeneous reaction
Stochastic modeling
Geochemistry

ABSTRACT

Mathematical models of advection–reaction phenomena rely on advective flow velocity and (bio) chemical reaction rates that are notoriously random. By using functional integral methods, we derive exact evolution equations for the probability density function (PDF) of the state variables of the advection–reaction system in the presence of random transport velocity and random reaction rates with rather arbitrary distributions. These PDF equations are solved analytically for transport with deterministic flow velocity and a linear reaction rate represented mathematically by a heterogeneous and strongly-correlated random field. Our analytical solution is then used to investigate the accuracy and robustness of the recently proposed large-eddy diffusivity (LED) closure approximation [1]. We find that the solution to the LED-based PDF equation, which is exact for uncorrelated reaction rates, is accurate even in the presence of strong correlations and it provides an upper bound of predictive uncertainty.

1. Introduction

The mathematical modeling of realistic advection–reaction phenomena involve many random parameters. For example, the dynamics of solute transport in an heterogeneous porous medium is significantly influenced by the epistemic uncertainty in the porosity distribution, advective (Darcy) flow velocity and (bio) chemical reaction rates [2]. These random fields render the governing equations of the advection–reaction system stochastic. A common approach to quantifying the statistical properties of the state variables of the system, e.g., the solute concentration, relies in modeling their probability density functions (PDFs) directly via deterministic equations. This has advantages over other uncertainty quantification methods, such as polynomial chaos [3–6], probabilistic collocation [7,8], perturbation methods [35–38], and generalized spectral decompositions [9–13]. In particular, PDF methods allow to directly ascertain the tails of probabilistic distributions thus facilitating the assessment of rare events and associated risks. This is in contrast to many other stochastic approaches that use the variance (or the standard deviation) of a system variable as a measure of predictive uncertainty. Another key advantage of PDF methods is that they do not suffer from the curse of dimensionality. Moreover, they can be used to tackle several open problems in stochastic dynamics such as discontinuities in parametric space [6] and long-term integration [14,15].

* Corresponding author. Tel.: +1 401 863 1217.
E-mail addresses: daniele_venturi@brown.edu, venturi.daniele@gmail.com (D. Venturi), george_karniadakis@brown.edu (G.E. Karniadakis).

0021-9991/$ - see front matter © 2013 Elsevier Inc. All rights reserved.
http://dx.doi.org/10.1016/j.jcp.2013.03.001

As is well known, in general it is not possible to determine an exact one-point (in space and time) PDF equation for the solution to an arbitrary partial differential equation. This is due to the fact that the solution to the PDE can be nonlocal in space and time.[1] However, a functional differential equation for the Hopf characteristic functional can always be determined [17–19], although effective analytical or numerical methods to solve it are still lacking. Moreover, the Hopf functional equation is equivalent to an infinite hierarchy of equations involving multi-point PDFs of increasing order [20–23].

First-order stochastic partial differential equations (SPDEs), such as the advection–reaction equation, are often amenable to exact treatment with PDF methods [1,24–26]. The main reason is that these equations can be reduced to a finite set of ordinary differential equations along the characteristic curves. This enables one to obtain an exact evolution equation for the *joint PDF* of the state variables and the external random fields appearing in the SPDE. In general, these random fields are high-dimensional, e.g., represented in terms of many random variables in a Karhunen–Loève expansion, and therefore the corresponding exact equation for the joint PDF is high-dimensional as well [27,26]. From a computational viewpoint this could be an issue despite the recent advances in numerical methods for high-dimensional problems such as proper generalized decomposition [28–30], sparse grid collocation [31,7] or functional ANOVA techniques [32–34].

A closure approximation can significantly reduce the number of parameters appearing in the PDF equation and therefore it can provide an effective computational tool that allows for an efficient integration. In particular, the large-eddy diffusivity (LED) closure for advection–reaction equations [1] has been shown to be effective for uncorrelated and weakly correlated random reaction rates. However, the performance of the LED-based PDF equations for strongly correlated reaction rates remains unexplored. Its investigation is the main objective of the present study. To this end, we consider the prototype problem proposed in [1] and obtain *analytical* solutions to the PDF equation for two different random reaction models. The analytical solutions will be employed as useful benchmark to test the accuracy and effectiveness of the LED closure.

This paper is organized as follows. In Section 2 we formulate the governing equations of advective-reactive transport in porous media and obtain an evolution law for the corresponding indicator function ([39, Ch. 3]). Section 2.2 presents the LED-based PDF equation for random advection–reaction transport. The exact evolution equation for the joint response-excitation PDF of the advection–reaction system is derived and discussed in Section 2.3. In Section 3 and Section 4 we compare the LED approximation with exact analytical results for a prototype advection–reaction problem involving linear reactions and strongly correlated random reaction rates. Finally, the main findings and their implications are summarized in Section 5. We also include two brief appendices, where we obtain analytical solutions to the equation for the joint response-excitation PDF and the advection–reaction equation in physical space.

2. Problem formulation

Let us consider the dimensionless form of the advection–reaction equation for a scalar concentration field $c(\boldsymbol{x}, t)$

$$\frac{\partial c}{\partial t} = -\nabla \cdot (\boldsymbol{u} c) + \mathrm{Da} f_\kappa(c), \quad f_\kappa(c) = -\alpha\kappa(c^\alpha - 1), \tag{1}$$

where $\boldsymbol{u}(\boldsymbol{x})$ is the dimensionless advective velocity; $\kappa(\boldsymbol{x})$ and α are the dimensionless reaction rate and the stoichiometric coefficient, respectively; and Da is the dimensionless Damköhler number.[2] The source function $f_\kappa(c)$ provides a macroscopic (continuum-scale) representation of a heterogeneous precipitation/dissolution reaction.[3] Eq. (1) is subject to suitable boundary conditions and the initial condition

$$c(\boldsymbol{x}, 0) = C_0(\boldsymbol{x}), \tag{2}$$

where $C_0(\boldsymbol{x})$ denotes the initial concentration.

Spatial heterogeneity and data scarcity render both advective velocity $\boldsymbol{u}(\boldsymbol{x})$ and reaction rate $\kappa(\boldsymbol{x})$ uncertain. To quantify the impact of this parametric uncertainty on predictions of concentration $c(\boldsymbol{x}, t)$, we treat these quantities as random fields, i.e., we consider $\boldsymbol{u}(\boldsymbol{x}; \omega)$ and $\kappa(\boldsymbol{x}; \omega)$, with ω indicating an element of the sample space in a suitable probability space. Additionally, we account for uncertainty in the initial concentration, i.e. we consider $C_0(\boldsymbol{x}; \omega)$. Available data or expert opinion (see, e.g., [24,25,1]) can be used to statistically characterize the random reaction rate $\kappa(\boldsymbol{x}; \omega)$; in this paper we will discuss two different models defined in terms of chi-squared and uniform random variables (see Section 3.1). Statistics of the

[1] Perhaps one of the simplest example is the solution to heat equation in a one-dimensional unbounded spatial domain for a random initial condition. In this case we have the random field [16]

$$\theta(x, t; \omega) = \int_{-\infty}^{\infty} \mathcal{G}(x, x' | t, 0) \theta_0(x'; \omega) dx'$$

where $\mathcal{G}$ denotes the Green function of the one-dimensional heat equation and $\theta_0(x, \omega)$ is the random initial temperature condition. Clearly, the statistical properties at location x and time $t + dt$ are influenced by the joint probability *functional* of $\theta(x, t; \omega)$ at time t, i.e. the joint probability density of $\theta(x, t; \omega)$ at *all* spatial points. Thus, no closed one-point (in space and time) PDF equation exists for the solution to the heat equation.

[2] We recall that $\mathrm{Da} \stackrel{\mathrm{def}}{=} D r_\kappa C_{\mathrm{eq}}^{\alpha-1} / V$, where D denotes the reference length, V the reference velocity, C_{eq} the deterministic equilibrium concentration, r_κ a scalar rescaling factor for the reaction rate κ and α the stoichiometric coefficient. The quantity r_κ can be, e.g., the mean reaction rate if this is a uniform (in space) stochastic process.

[3] It is worthwhile emphasizing that the methodology described in this paper is also applicable to other types of chemical reactions, defined in terms of different $f_\kappa(c)$.

macroscopic flow velocity $\boldsymbol{u}(\boldsymbol{x};\omega)$, including its spatially varying mean $\langle \boldsymbol{u}(\boldsymbol{x};\omega)\rangle$ and correlation $\langle u_i(\boldsymbol{x};\omega)u_j(\boldsymbol{y};\omega)\rangle$ $(i,j=1,2,3)$, can be determined by solving the flow equations with random hydraulic conductivity or random initial and boundary conditions (e.g., [40,41]).

2.1. Equations for the indicator function

Let us consider the function

$$\Pi(a,\boldsymbol{x},t;\omega) \equiv \delta(a - c(\boldsymbol{x},t;\omega)), \tag{3}$$

where $\delta(\cdot)$ is the Dirac delta and a is a deterministic value that the random concentration c can take at a space-time point $(\boldsymbol{x},t)$. The ensemble average (over random c) of Π is the one-point (in space and time) PDF of the concentration $c(\boldsymbol{x},t;\omega)$,

$$p^{(a)}_{c(\boldsymbol{x},t)} \stackrel{\text{def}}{=} \langle \Pi(a,\boldsymbol{x},t;\omega)\rangle. \tag{4}$$

By using elementary properties of the Dirac delta function [42], it is easy to show that $\Pi(a,\boldsymbol{x},t;\omega)$ satisfies a linear advection equation (see [39, Ch. 3])

$$\frac{\partial \Pi}{\partial t} + \nabla\cdot(\boldsymbol{u}\Pi) = -\mathrm{Da}\frac{\partial[f_\kappa(a)\Pi]}{\partial a}. \tag{5}$$

Following [1], we introduce a four-dimensional space with coordinates $\tilde{\boldsymbol{x}} = (x_1,x_2,x_3,x_4\equiv a)$, in which the gradient operator and the velocity field are defined as

$$\tilde{\nabla} \stackrel{\text{def}}{=} \left(\frac{\partial}{\partial x_1},\frac{\partial}{\partial x_2},\frac{\partial}{\partial x_3},\frac{\partial}{\partial x_4}\equiv\frac{\partial}{\partial a}\right), \quad \tilde{\boldsymbol{u}} \stackrel{\text{def}}{=} (u_1,u_2,u_3,u_4\equiv \mathrm{Da}f_\kappa(a)). \tag{6}$$

This allows us to rewrite (5) in the compact form

$$\frac{\partial \Pi}{\partial t} + \tilde{\nabla}\cdot(\tilde{\boldsymbol{u}}\Pi) = 0. \tag{7}$$

Stochastic averaging of this equation yields a one-point PDF equation

$$\frac{\partial p^{(a)}_{c(x,t)}}{\partial t} = -\tilde{\nabla}\cdot\left[\langle\tilde{\boldsymbol{u}}\rangle p^{(a)}_{c(x,t)}\right] - \tilde{\nabla}\cdot\langle\tilde{\boldsymbol{u}}'\Pi\rangle, \tag{8}$$

where the prime denotes the fluctuating part of the Reynolds decomposition of $\tilde{\boldsymbol{u}}$. The cross-correlation term $\langle\tilde{\boldsymbol{u}}'\Pi\rangle$ in (8) requires a closure approximation. Over the years, and in different contexts, many closures (e.g., [43–45]) have been proposed in order to express $\langle\tilde{\boldsymbol{u}}'\Pi\rangle$ in terms of the one-point PDF $p^{(a)}_{c(x,t)}$. One of these methods is described below.

2.2. Large-eddy diffusivity (LED) approximation

The Large-eddy diffusivity (LED) approximation [1] is a phenomenological closure that allows one to replace the PDF Eq. (8) with a Fokker–Planck type equation

$$\frac{\partial p^{(a)}_{c(\boldsymbol{x},t)}}{\partial t} = -\frac{\partial\left[U_i p^{(a)}_{c(\boldsymbol{x},t)}\right]}{\partial\tilde{x}_i} + \frac{\partial}{\partial\tilde{x}_j}\left[D_{ij}\frac{\partial p^{(a)}_{c(\boldsymbol{x},t)}}{\partial\tilde{x}_i}\right], \quad i,j=1,\ldots,4. \tag{9}$$

The "effective diffusivity" D_{ij} and the "effective velocity" $\boldsymbol{U}$ are defined as

$$D_{ij}(\tilde{\boldsymbol{x}},t) \stackrel{\text{def}}{=} \int_0^t\int_{\tilde{\Omega}}\langle\tilde{u}_i'(\tilde{\boldsymbol{x}})\tilde{u}_j'(\tilde{\boldsymbol{y}})\mathcal{G}(\tilde{\boldsymbol{x}},\tilde{\boldsymbol{y}},t-\tau)\rangle\mathrm{d}\tilde{\boldsymbol{y}}\mathrm{d}\tau, \quad i,j=1,\ldots,4, \tag{10}$$

$$\boldsymbol{U}(\tilde{\boldsymbol{x}},t) \stackrel{\text{def}}{=} \langle\tilde{\boldsymbol{u}}\rangle - \mathrm{Da}\int_0^t\int_{\tilde{\Omega}}\langle\tilde{\boldsymbol{u}}'(\tilde{\boldsymbol{x}})\frac{\partial f_\kappa'(\tilde{\boldsymbol{y}})}{\partial y_4}\mathcal{G}(\tilde{\boldsymbol{x}},\tilde{\boldsymbol{y}},t-\tau)\rangle\mathrm{d}\tilde{\boldsymbol{y}}\mathrm{d}\tau, \tag{11}$$

where $\tilde{u}_j'(\tilde{\boldsymbol{y}})$ denotes the velocity fluctuation arising from the Reynolds decomposition of the four-dimensional random velocity as $\tilde{\boldsymbol{u}} = \langle\tilde{\boldsymbol{u}}\rangle + \tilde{\boldsymbol{u}}'$, and $\mathcal{G}$ is the random Green function associated with (7). The latter is defined as a solution of

$$\frac{\partial\mathcal{G}}{\partial\tau} + \tilde{\boldsymbol{u}}\cdot\tilde{\nabla}\mathcal{G} = -\delta(\tilde{\boldsymbol{x}}-\tilde{\boldsymbol{y}})\delta(t-\tau), \tag{12}$$

subject to the appropriate homogeneous initial and boundary conditions. To render the diffusion tensor (10) and effective velocity (11) computable, we approximate the third-moments in their integrands as follows

$$D_{ij}(\tilde{\boldsymbol{x}},t) \simeq \int_0^t\int_{\tilde{\Omega}}\langle\tilde{u}_i'(\tilde{\boldsymbol{x}})\tilde{u}_j'(\tilde{\boldsymbol{y}})\rangle G(\tilde{\boldsymbol{x}},\tilde{\boldsymbol{y}},t-\tau)\mathrm{d}\tilde{\boldsymbol{y}}\mathrm{d}\tau, \tag{13}$$

$$\boldsymbol{U}(\tilde{\boldsymbol{x}},t) \simeq \langle \tilde{\boldsymbol{u}} \rangle - \mathrm{Da} \int_0^t \int_{\tilde{\Omega}} \langle \tilde{\boldsymbol{u}}'(\tilde{\boldsymbol{x}}) \kappa'(\tilde{\boldsymbol{y}}) \rangle \frac{\partial f_\alpha(y_4)}{\partial y_4} G(\tilde{\boldsymbol{x}},\tilde{\boldsymbol{y}},t-\tau) \mathrm{d}\tilde{\boldsymbol{y}} \mathrm{d}\tau. \tag{14}$$

Here $f_\alpha(y_4) \stackrel{\text{def}}{=} -\alpha(y_4^\alpha - 1)$ and G is a deterministic Green function defined as a solution to the deterministic advection equation

$$\frac{\partial G}{\partial \tau} + \langle \tilde{\boldsymbol{u}} \rangle \cdot \tilde{\nabla} G = -\delta(\tilde{\boldsymbol{x}} - \tilde{\boldsymbol{y}}) \delta(t-\tau). \tag{15}$$

This approximation has been shown to be effective if $p^{(a)}_{c(\boldsymbol{x},t)}$ varies slowly in time and space relatively to $\tilde{\boldsymbol{u}}$.

2.3. Exact joint PDF equation

Let us assume that the random coefficients $\kappa(\boldsymbol{x};\omega)$ and $\boldsymbol{u}(\boldsymbol{x};\omega)$ can be represented, with a given degree of accuracy, with finite series

$$\kappa(\boldsymbol{x};\omega) = \sum_{j=1}^{N} \chi_j(\omega) \phi_j(\boldsymbol{x}), \quad \boldsymbol{u}(\boldsymbol{x};\omega) = \sum_{j=1}^{M} \eta_j(\omega) \boldsymbol{\varphi}_j(\boldsymbol{x}), \tag{16}$$

where $\boldsymbol{\chi}(\omega) = \{\chi_1,\ldots,\chi_N\}$ and $\boldsymbol{\eta}(\omega) = \{\eta_1,\ldots,\eta_M\}$ are two sets of random variables with known joint probability density function. Then, in analogy with (4), the joint PDF of the concentration field $c(\boldsymbol{x},t;\omega)$ and the random vectors $\boldsymbol{\chi}(\omega)$ and $\boldsymbol{\eta}(\omega)$ can be expressed as (e.g., [20])

$$p^{(a,\boldsymbol{b},\boldsymbol{z})}_{c(\boldsymbol{x},t)\boldsymbol{\chi}\boldsymbol{\eta}} = \langle \delta(a - c(\boldsymbol{x},t;\omega)) \prod_{j=1}^{N} \delta(b_j - \chi_j(\omega)) \prod_{k=1}^{M} \delta(z_k - \eta_k(\omega)) \rangle, \tag{17}$$

where the elements of sets $\boldsymbol{b} = \{b_1,\ldots,b_N\}$ and $\boldsymbol{z} = \{z_1,\ldots,z_M\}$ represent deterministic values that the corresponding random elements of the sets $\boldsymbol{\chi}(\omega)$ and $\boldsymbol{\eta}(\omega)$ can take on, and the stochastic average is with respect to the joint probability functional of the variables $\boldsymbol{\chi}(\omega)$ and $\boldsymbol{\eta}(\omega)$ and all the other input processes such as random boundary and initial conditions. Differentiating (17) with respect to time t and making use of (1) yields

$$\begin{aligned} \frac{\partial P}{\partial t} &= -\frac{\partial}{\partial a} \langle \delta(a-c) \frac{\partial c}{\partial t} \prod_{j=1}^{N} \delta(b_j - \chi_j) \prod_{k=1}^{M} \delta(z_k - \eta_k) \rangle \\ &= -\frac{\partial}{\partial a} \langle \delta(a-c) [-\nabla \cdot (\boldsymbol{u}c) + \mathrm{Da} f_\kappa(c)] \frac{\partial c}{\partial t} \prod_{j=1}^{N} \delta(b_j - \chi_j) \prod_{k=1}^{M} \delta(z_k - \eta_k) \rangle, \end{aligned} \tag{18}$$

where P is a shorthand notation for the multi-dimensional joint PDF (17). Substituting (16) into (18), we find that P satisfies a linear advection equation in the variables $(t,\boldsymbol{x},a)$ with $(N+M)$ parameters,

$$\frac{\partial P}{\partial t} = \frac{\partial}{\partial a} \left(a P \sum_{j=1}^{M} z_j \nabla \cdot \boldsymbol{\varphi}_j \right) - \nabla P \cdot \left(\sum_{j=1}^{M} z_j \boldsymbol{\varphi}_j \right) - \mathrm{Da} \frac{\partial}{\partial a} \left((a^\alpha - 1) P \sum_{j=1}^{N} b_j \phi_j \right). \tag{19}$$

The one-point PDF of the concentration c is obtained by marginalizing P with respect to all the parameters $\boldsymbol{b}$ and $\boldsymbol{z}$,

$$p^{(a)}_{c(\boldsymbol{x},t)} = \int_{-\infty}^{\infty} \cdots \int_{-\infty}^{\infty} p^{(a,\boldsymbol{b},\boldsymbol{z})}_{c(\boldsymbol{x},t)\boldsymbol{\chi}\boldsymbol{\eta}} \mathrm{d}b_1 \ldots \mathrm{d}b_N \mathrm{d}z_1 \ldots \mathrm{d}z_M. \tag{20}$$

The corresponding (integro-differential) evolution equation for $p^{(a)}_{c(\boldsymbol{x},t)}$ can be obtained by integrating (19) with respect to the variables $\boldsymbol{b}$ and $\boldsymbol{z}$.

The following points are worthwhile emphasizing. First, apart from the decomposition of the random coefficients $\boldsymbol{u}$ and κ into the finite-term series (16), the evolution equation for the joint PDF (19) is exact, i.e, it requires no closure approximations. Second, the parametric space of the joint PDF (19) is significantly higher than that of the LED-based PDF Eq. (9). Third, the sequence of steps leading to the PDF Eqs. (9) and (19) can be applied to quantify parametric uncertainty in more general nonlinear first-order PDEs of the form $\partial c/\partial t + \mathcal{P}(c,t,\boldsymbol{x},\boldsymbol{\chi}) \cdot \nabla_{\boldsymbol{x}} c = \mathcal{Q}(c,t,\boldsymbol{x},\boldsymbol{\eta})$ [26,46].

3. Comparison between LED-based and exact PDF equations

To elucidate the salient features of the two approaches to derivation of PDF equations, we consider a one-dimensional advection-reaction Eq. (1) with a linear reaction term ($\alpha = 1$). Mass conservation requires the dimensionless advection velocity u to be constant and deterministic (e.g., [1], §4). Without loss of generality, we set $u = 1$ so that the reaction rate $\kappa(\boldsymbol{x})$ is the only source of uncertainty. Under these conditions, (1) reduces to

$$\frac{\partial c}{\partial t} = -\frac{\partial c}{\partial x} - \mathrm{Da}\ \kappa(x;\omega)(c-1) \quad x \in [0,L]. \tag{21}$$

We supplement (21) with the following boundary and initial conditions

$$c(0,t;\omega)=0, \quad c(x,0;\omega)=0. \tag{22}$$

To ensure the well-posedness of the initial-boundary value problem (21), (22), the characteristic curves [47] of (21) arising from the initial-boundary data should not intersect each others. In other words, the characteristic curves originating from $t=0$ should not intersect the ones from $x=0$ (see Section 3.4 for more details).

3.1. Modeling of the random reaction rate

The previous analyzes (e.g., [24,25]) treated the random reaction rate $\kappa(x;\omega)$ as a statistically homogeneous multi-variate log-normal field. In this paper we will employ two alternative statistical models of $\kappa(x;\omega)$, both of which are described below.

3.1.1. Reaction rate model based on chi-squared random variables

Let us represent the random reaction rate $\kappa(x;\omega)$ on the one-dimensional interval $[0,L]$ with a finite-term series

$$\kappa(x;\omega)=\sum_{j=1}^{N}\chi_j(\omega)\phi_j(x), \quad x\in[0,L]. \tag{23}$$

The modes $\phi_k(x)$ and the random variables $\chi_k(\omega)$ have to be selected in a way that ensures that $\kappa(x;\omega)$ remains positive with probability one. We achieve this requirement by taking $\chi_k(\omega)$ to be independent *chi-squared* random variables. This yields a random reaction rate whose one-point distribution function can be represented in terms of an infinite series of incomplete gamma integrals [48] or other series involving normal variables [49–52]. Among several possible choices, we consider the representation given by an infinite linear combination of chi-squared distribution functions with an arbitrary scale parameter $\beta>0$ (e.g., Theorem 2 in [49], or §6 in [50]). Let us denote the distribution function of $\kappa(x;\omega)$ by

$$\mathcal{P}^{(a)}_{\kappa(x)} \overset{\text{def}}{=} \Pr\left[\sum_{j=1}^{N}\chi_j(\omega)\phi_j(x)\leqslant a\right]. \tag{24}$$

For all x such that $\phi_j(x)\neq 0$ $(j=1,\dots,N)$,[4] the (central) chi-squared distribution function with N degrees of freedom is given by

$$\mathcal{P}^{(a)}_{\kappa(x)}=\sum_{j=0}^{\infty}c_j(x)F_{N+2j}\left(\frac{a}{\beta}\right), \quad F_n(a)=\frac{1}{2^{n/2}\Gamma(n/2)}\int_0^a \mathrm{e}^{-y/2}y^{n/2-1}\mathrm{d}y, \tag{25}$$

where the coefficients $c_j(x)$ satisfy the recursion relationship

$$c_j(x)=\frac{1}{2j}\sum_{r=0}^{j-1}g_{j-r}(x)c_r(x), \quad c_0=\prod_{i=1}^{N}\left(\frac{\beta}{\phi_i(x)}\right)^{1/2}, \quad g_m(x)=\sum_{i=1}^{N}\left(1-\frac{\beta}{\phi_i(x)}\right)^m. \tag{26}$$

The series (25) converges *uniformly* in every finite interval of a [49]. Differentiating the distribution function (25) with respect to a, we obtain the one-point PDF of the random reaction rate (23),

$$p^{(a)}_{\kappa(x)}=\frac{1}{\beta}\sum_{j=0}^{\infty}c_j(x)q_{N+2j}\left(\frac{a}{\beta}\right), \quad \text{where } q_n(s)=\frac{\mathrm{e}^{-s/2}s^{n/2-1}}{2^{n/2}\Gamma(n/2)}. \tag{27}$$

The correlation structure of the random field (23) is obtained as

$$\langle\kappa(x;\omega)\kappa(y;\omega)\rangle=3\sum_{i=1}^{N}\phi_i(x)\phi_i(y)+\sum_{\substack{i,j=1\\ i\neq j}}^{N}\phi_i(x)\phi_j(y), \tag{28}$$

while the covariance function is

$$C_\kappa(x,y)\overset{\text{def}}{=}\langle\kappa(x;\omega)\kappa(y;\omega)\rangle-\langle\kappa(x;\omega)\rangle\langle\kappa(y;\omega)\rangle=2\sum_{i=1}^{N}\phi_i(x)\phi_i(y). \tag{29}$$

Among many possible choices of the bases functions $\phi_j(x)$, in this paper we consider

$$\phi_j(x)=\frac{1}{\lambda^j}\sin\left(\frac{j}{L}x\right)^2, \quad \lambda>1. \tag{30}$$

[4] The results presented in [49] are valid in the more general case of arbitrary *non-negative* quadratic forms of standard Gaussian variables. This means that they include also the cases where some of the ϕ_i in (23) are zero. In this circumstance we can simply remove those terms from the series (23) and then apply formula (25).

The corresponding random samples of $\kappa(x;\omega)$ and its covariance are shown in Fig. 1 for several λ. Note that the random reaction rate is positive with probability 1 (as it should be), and at $x = 0$ it is always zero by construction. Fig. 2 exhibits the relative L_1 norm of each term in the series expansion (23). This quantity is defined as

$$\mu_k \stackrel{\text{def}}{=} \frac{e_k}{\sum_j e_j}, \quad e_k \stackrel{\text{def}}{=} \int_0^L |\phi_k(x)| \mathrm{d}x. \tag{31}$$

It represents the relative contribution of each term in the representation of the random field $\kappa(x;\omega)$ as a function of the parameter λ. Substituting 30 into (31) yields

$$e_k = \frac{2k - \sin(2k)}{4k\lambda^k/L}. \tag{32}$$

Let

$$N = \max_k [\mu_k] \geqslant \tau \tag{33}$$

define the dimensionality of the random field $\kappa(x;\omega)$, i.e., the number of random variables in the series (23) that is required to reach a certain threshold τ. The table in Fig. 2 shows how the dimensionality N increases with the decreasing values of λ,

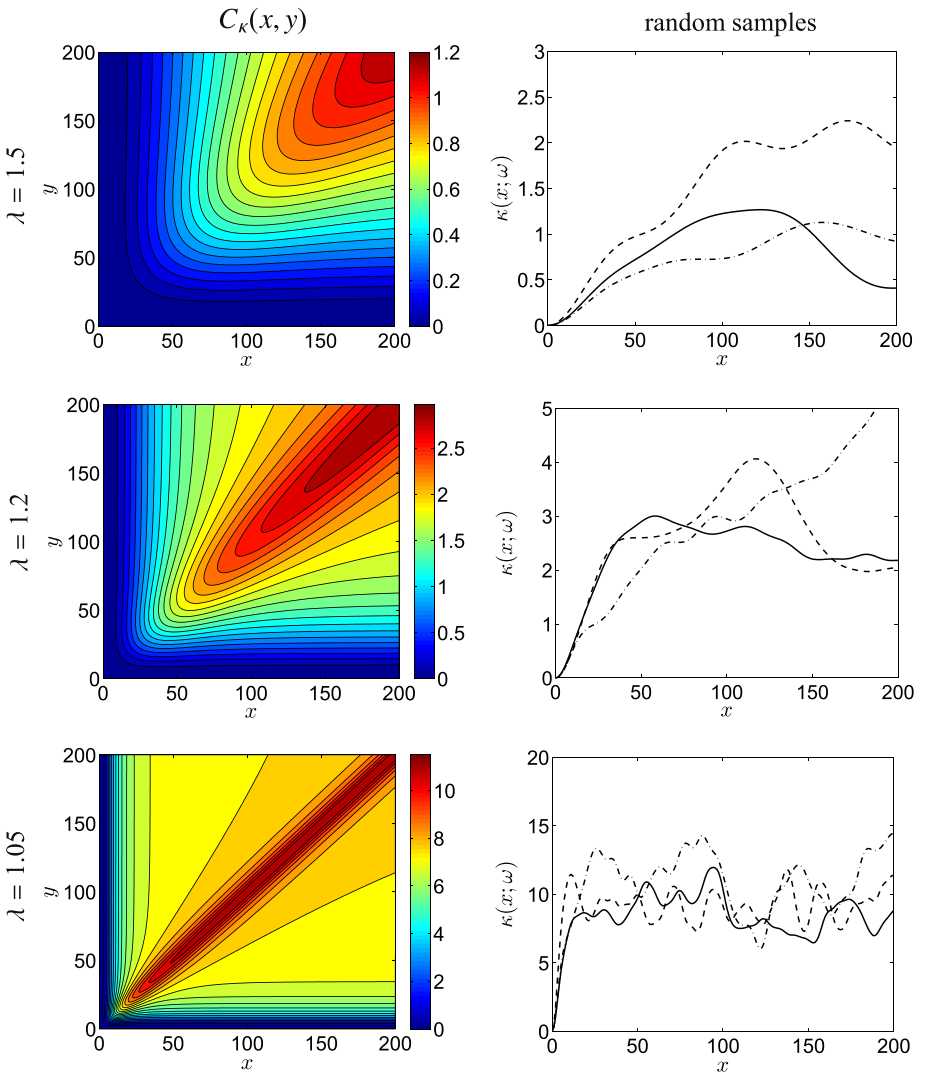

Fig. 1. Covariance function (28) (left column) and random samples of the reaction rate (23) (right column) for different values of the parameter λ (see Eq. (30)).

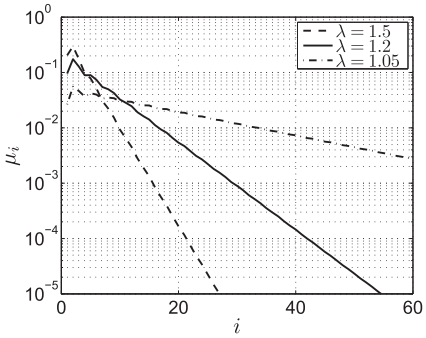

Dimensionality of the random reaction rate (23) for $\tau = 0.05\%$ (see Eq. (33))

λ	N
100	2
10	4
4	6
2	11
1.5	17
1.2	33
1.1	55
1.05	94

Fig. 2. Relative L_1 norm (31) of each term in the series representation of the random reaction rate (23). Shown are results for different λ (see Eq. (30)). The dimensionality of the random reaction rate, i.e., number of random variables in Eq. (23), is shown in the table for a threshold set at $\tau = 0.05\%$.

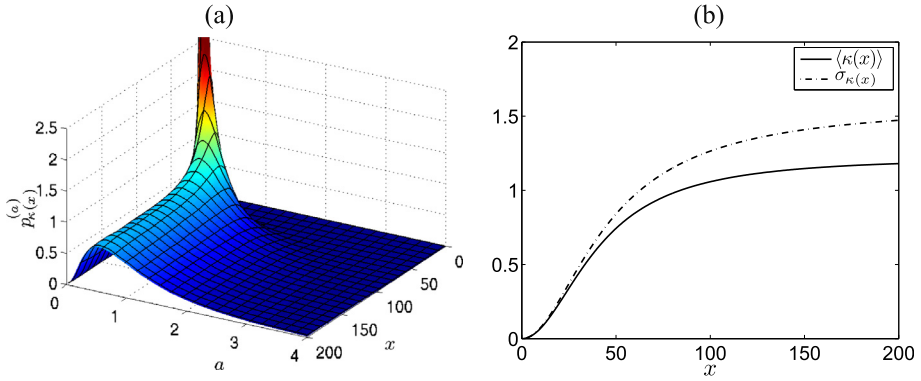

Fig. 3. (a) One-point probability density function (27) of the random reaction rate $\kappa(x;\omega)$ for $\lambda = 1.5$. (b) Mean and standard deviation of $\kappa(x;\omega)$.

for the threshold $\tau = 0.05\%$. Fig. 3 provides an example of the one-point PDF (27), the mean, and standard deviation of $\kappa(x;\omega)$ corresponding to $\lambda = 1.5$.

3.1.2. Reaction rate model based on uniform random variables

The second finite-series representation the random reaction rate $\kappa(x;\omega)$ is based on a truncated Karhunen–Loève expansion

$$\kappa(x;\omega) = K + \frac{\sqrt{3}\sigma_\kappa}{\sqrt{2\ell}} \sum_{j=1}^{N} \sqrt{\theta_j}\zeta_j(\omega)\eta_j(x), \tag{34}$$

where K is a positive constant, and $\zeta_j(\omega)$ are zero-mean independent *uniform* random variables in $[-1, 1]$. The quantities θ_j and $\eta_j(x)$ denote, respectively, the eigenvalues and the eigenfunctions of the exponential covariance function

$$C_\kappa(x,y) = \frac{\sigma_\kappa^2}{2\ell} \mathrm{e}^{-|x-y|/\ell}, \tag{35}$$

where ℓ is the correlation length.[5] The factor $\sqrt{3}$ on the right-hand-side of (34) reflects the choice of $\langle \zeta_j^2 \rangle = 1/3$ and ensures that (34) and (35) are consistent. The eigenvalues θ_j and eigenfunctions $\eta_j(x)$ of the exponential correlation function (35) are given by (e.g., [53])

$$\theta_j = \frac{2\ell}{\ell^2 z_j^2 + 1}, \quad \eta_j(x) = \frac{z_j \ell}{A_j} \cos(z_j x) + \frac{1}{A_j} \sin(z_j x), \tag{36}$$

where z_j are zeros of the transcendental equation

$$\left(z_i^2 - \frac{1}{\ell^2}\right) \tan(z_i L) - 2\frac{z_i}{\ell} = 0 \tag{37}$$

and

[5] Note that $C_\kappa(x,y)$ is an element of a delta sequence that converges to $\sigma_\kappa^2 \delta(x-y)$ as $\ell \to 0$.

$$A_j \stackrel{\text{def}}{=} \sqrt{L\frac{1+z_j^2\ell^2}{2}+\frac{z_j^2\ell^2-1}{4z_j}\sin(2z_jL)+\ell\frac{1-\cos(2z_jL)}{2}}. \tag{38}$$

In analogy with the previous section, we define the relative spectrum Θ_j and the dimensionality N of the Karhunen–Loève expansion (34) for a given threshold level τ as

$$\Theta_j = \frac{\theta_j}{\sum_k \theta_k}, \quad N = \max_i[\Theta_i] > \tau. \tag{39}$$

Fig. 4 shows Θ_j and N for $\tau = 0.05\%$ and different correlation lengths ℓ. For each correlation length ℓ, the constant K in (34) can be selected to ensure that $\kappa(x;\omega)$ is *positive with probability one* (Fig. 5). The lower bound of $K\sqrt{2\ell}/(\sqrt{3}\sigma_\kappa)$ in Fig. 5 is valid for uniform variables in $[-1,1]$. It is obtained numerically by first sampling (34) and then computing the minimum over all the realizations. For other types of random variables the bounds in Fig. 5 are different.
Several realization of the random reaction rate for different correlation lengths and perturbation amplitude $\sigma_\kappa\sqrt{3}/\sqrt{2\ell} = 0.25$ are shown in Fig. 6. The value of K in (34) is selected in order to satisfy the positivity condition. The one-point PDF of the Karhunen–Loève series (34) with uniformly distributed ζ_i has a nontrivial mathematical expression [54,55]; it is plotted in Fig. 7 for different correlation lengths ℓ. Note that as $\ell \to 0$ (i.e. for $N \to \infty$), the PDF becomes Gaussian, in agreement with the central limit theorem. In other words, the random reaction rate (34) becomes *Gaussian white noise* as $\ell \to 0$.

3.2. Exact joint PDF equation

The joint PDF equation for the random concentration $c(x,t;\omega)$ whose dynamics is governed by (21) with random reaction rate (23) is (see Section 2.3)

$$\frac{\partial P}{\partial t} = -\frac{\partial P}{\partial x} - \mathrm{Da}\frac{\partial[(1-a)P]}{\partial a}\sum_{i=1}^{N}\phi_i(x)b_i, \tag{40}$$

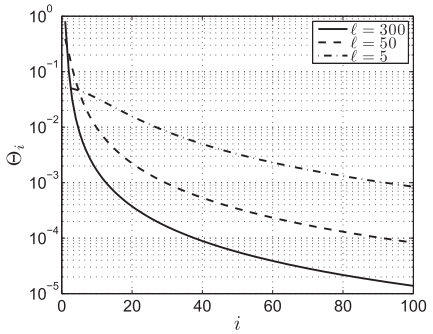

Dimensionality of the random reaction rate for $\tau = 0.05\%$

ℓ	N
1000	9
300	17
100	29
50	41
5	127
1	278
0.1	728

Fig. 4. Spectral decay of the Karhunen–Loève expansion (34) as a function of the correlation length ℓ. The covariance of the random reaction rate is assumed to be exponential. The table on the right shows the number of expansion terms in (34) for $L = 200$ and an energy threshold set at $\tau = 0.05\%$.

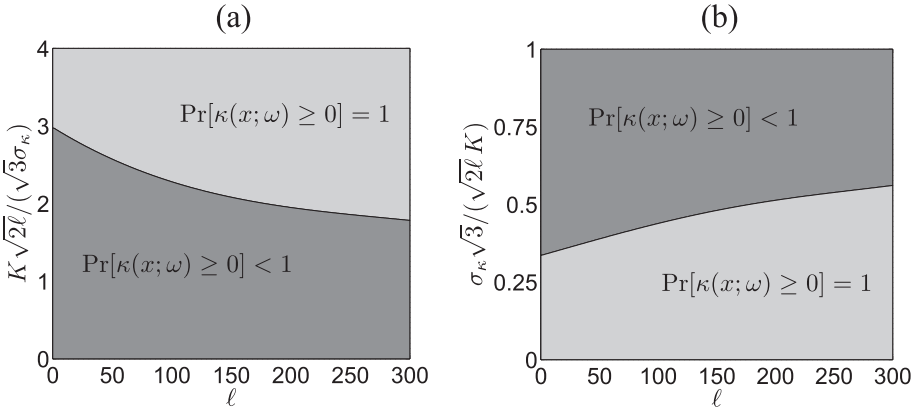

Fig. 5. (a) Lowest values of the constant $K\sqrt{2\ell}/(\sqrt{3}\sigma_\kappa)$ for which the exponentially correlated random reaction rate (34) is positive with probability one. (b) Same as figure (a) but here we show $\sigma_\kappa\sqrt{3}/(K\sqrt{2\ell})$ versus ℓ. These plots are valid when the random variables $\zeta_k(\omega)$ appearing in (34) are uniform in $[-1,1]$ and independent to each other.

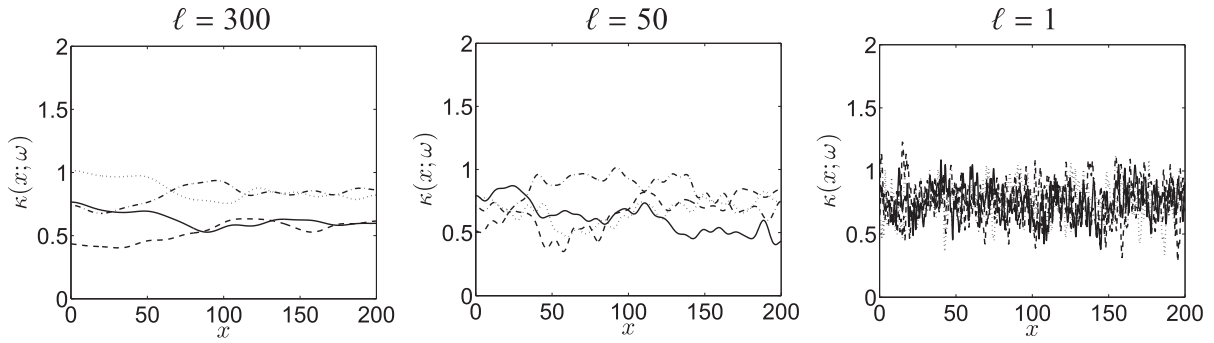

Fig. 6. Samples of the exponentially correlated random reaction rate (34) for $K = 0.75$ and $\sigma_\kappa\sqrt{3}/\sqrt{2\ell} = 0.25$. We show results corresponding to different correlation lengths. Note that with this choice of parameters the the positivity condition of Fig. 5 is satisfied for all $\ell > 1$ since $K\sqrt{2\ell}/(\sqrt{3}\sigma_\kappa) = 3$.

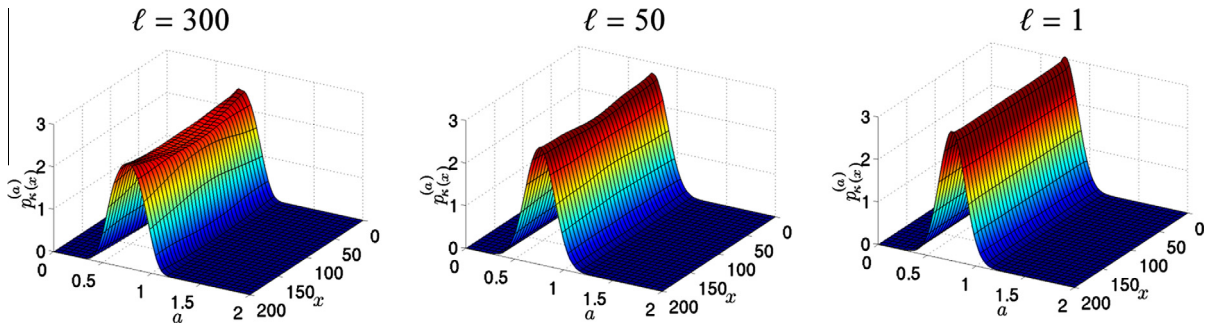

Fig. 7. One-point PDF of the random reaction rate (34) for $\sigma_\kappa\sqrt{3}/\sqrt{2\ell} = 0.25$, $K = 0.75$, and different correlation lengths ℓ.

where P is a shorthand notation for

$$p^{(a,\boldsymbol{b})}_{c(x,t)\boldsymbol{\chi}} = \langle \delta(a - c(x,t;\omega)) \prod_{k=1}^{N} \delta(b_k - \chi_k(\omega)) \rangle. \tag{41}$$

Integration of (40) with respect to $\boldsymbol{b} = \{b_1, \ldots, b_N\}$ yields an evolution equation for the one-point PDF of the random concentration field,

$$\frac{\partial p^{(a)}_{c(x,t)}}{\partial t} = -\frac{\partial p^{(a)}_{c(x,t)}}{\partial x} - \mathrm{Da}\frac{\partial}{\partial a}\left[(1-a)\sum_{i=1}^{N}\phi_i(x)\int_{-\infty}^{\infty} b_i p^{(a,b_i)}_{c(x,t)\chi_i}\,\mathrm{d}b_i\right]. \tag{42}$$

This equation remains unclosed since the dynamics of the one-point PDF $p^{(a)}_{c(x,t)}$ depends on N joint PDFs $p^{(a,b_i)}_{c(x,t)\chi_i}$. Auxiliary conditions for the joint PDF Eq. (40) are derived from the initial and boundary conditions (22). Taking the deterministic concentration outside the averaging operator in the definition (41), we obtain the boundary and initial conditions[6]

$$p^{(a,\boldsymbol{b})}_{c(0,t)\boldsymbol{\chi}} = \delta(a-0)p^{(\boldsymbol{b})}_{\boldsymbol{\chi}}, \quad p^{(a,\boldsymbol{b})}_{c(x,0)\boldsymbol{\chi}} = \delta(a-0)p^{(\boldsymbol{b})}_{\boldsymbol{\chi}}. \tag{45}$$

Assignment of boundary conditions with respect to a is nontrivial. If the joint PDF $p^{(a,\boldsymbol{b})}_{c(x,t)\boldsymbol{\chi}}$ were defined on the interval $-\infty < a < \infty$, then a natural boundary condition to use would be $p^{(\pm\infty,\boldsymbol{b})}_{c(x,t)\boldsymbol{\chi}} = 0$. However, it follows from the problem formulation (21), (22) that $c(x,t;\omega) \in [0,1]$ with probability 1. This, in turn, implies that both the joint PDF Eq. (40) and its single-point counterpart (42) are defined on the compact support $a \in [0,1]$ for which PDF boundary conditions are not clearly defined. In the following section, we remove this ambiguity by reformulating the problem in terms of cumulative density

[6] Sometimes it may not be convenient to have a Dirac delta function at the boundary or at the initial condition of a PDE. In these circumstances one can first parametrize such conditions by using, e.g., an element of a delta sequence ([42, p. 58]) $\Delta_\epsilon(a)$, e.g.,

$$\Delta_\epsilon(a) = \frac{1}{\Gamma(q/2)2^{q/2}\epsilon}\left(\frac{a}{\epsilon}\right)^{q/2} e^{-a/(2\epsilon)} \quad (q \in \mathbb{N}), \quad \lim_{\epsilon\to 0}\Delta_\epsilon(a) = \delta(a), \tag{43}$$

and then compute the solution to the PDE equation corresponding to the regularized boundary and initial conditions

$$\hat{p}^{(a,b_1,\cdots,b_N)}_{c(0,t)\chi_1\cdots\chi_N} = \Delta_\epsilon(a)p^{(b_1,\cdots,b_N)}_{\chi_1\cdots\chi_N}, \quad \hat{p}^{(a,b_1,\cdots,b_N)}_{c(x,0)\chi_1\cdots\chi_N} = \Delta_\epsilon(a)p^{(b_1,\cdots,b_N)}_{\chi_1\cdots\chi_N}. \tag{44}$$

Once the solution to the regularized problem is available, then we set $\epsilon \to 0$ to obtain the desired solution.

functions instead of PDFs. In appendix A, we use the method of characteristics (e.g., [47]) to analytically solve the joint PDF Eq. (40) subject to the auxiliary conditions (45).

3.3. LED-based PDF equation

For the problem under consideration, the general PDF Eq. (9) reduces to

$$\frac{\partial p^{(a)}_{c(x,t)}}{\partial t} = -\frac{\partial p^{(a)}_{c(x,t)}}{\partial x} - \frac{\partial\left[U_4 p^{(a)}_{c(x,t)}\right]}{\partial a} + \frac{\partial}{\partial a}\left[D_{44}\frac{\partial p^{(a)}_{c(x,t)}}{\partial a}\right], \tag{46}$$

where the diffusion coefficient and the effective velocity are given by [1]

$$D_{44}(x,a,t) = \mathrm{Da}^2(a-1)^2\begin{cases}\int_0^t C_\kappa(x,x-b)\mathrm{e}^{2b\mathrm{Da}}\mathrm{d}b & t \leqslant T(a)\\ \int_0^T C_\kappa(x,x-b)\mathrm{e}^{2b\mathrm{Da}}\mathrm{d}b & t > T(a)\end{cases} \tag{47}$$

and

$$U_4(x,a,t) = \langle\kappa(x;\omega)\rangle\mathrm{Da}(1-a) - \mathrm{Da}^2(a-1)\begin{cases}\int_0^t C_\kappa(x,x-b)e^{b\mathrm{Da}}\mathrm{d}b & t \leqslant T(a)\\ \int_0^T C_\kappa(x,x-b)e^{b\mathrm{Da}}\mathrm{d}b & t > T(a)\end{cases}, \tag{48}$$

with

$$T(a) \overset{\mathrm{def}}{=} \frac{1}{\mathrm{Da}}\ln\left(\frac{1}{1-a}\right). \tag{49}$$

Eq. (46), together with the boundary and initial conditions

$$p^{(a)}_{c(x,0)} = \delta(a), \quad p^{(a)}_{c(0,t)} = \delta(a), \tag{50}$$

can be rewritten in terms of the cumulative distribution function

$$\mathcal{P}^{(a)}_{c(x,t)} = \int_0^a p^{(a')}_{c(x,t)}da'. \tag{51}$$

The result is

$$\frac{\partial \mathcal{P}^{(a)}_{c(x,t)}}{\partial t} = -\frac{\partial \mathcal{P}^{(a)}_{c(x,t)}}{\partial x} - U_4(x,a,t)\frac{\partial \mathcal{P}^{(a)}_{c(x,t)}}{\partial a} + D_{44}(x,a,t)\frac{\partial^2 \mathcal{P}^{(a)}_{c(x,t)}}{\partial a^2} + J(x,a,t)|_{a=0}, \tag{52}$$

where

$$J(x,a,t) \overset{\mathrm{def}}{=} U_4(x,a,t)\frac{\partial \mathcal{P}^{(a)}_{c(x,t)}}{\partial a} - D_{44}(x,a,t)\frac{\partial^2 \mathcal{P}^{(a)}_{c(x,t)}}{\partial a^2} \tag{53}$$

denotes the *probability current*. Eq. (52) is second-order in a and first-order in x and t. Therefore, it requires two additional conditions in a, namely,

$$\mathcal{P}^{(0)}_{c(x,t)} = 0, \quad \mathcal{P}^{(1)}_{c(x,t)} = 1, \tag{54}$$

one condition in x

$$\mathcal{P}^{(a)}_{c(0,t)} = 1 \tag{55}$$

and the initial condition

$$\mathcal{P}^{(a)}_{c(x,0)} = 1. \tag{56}$$

Both the effective velocity and the diffusion tensor decrease as the Damköhler number Da becomes smaller. In the limit $\mathrm{Da} \to 0, U_4 \to 0$ and $D_{44} \to 0$. In this limit, the LED-based PDF Eq. (46) self-consistently reduces to pure linear advection.

3.3.1. Coefficients for the chi-squared reaction rate model

For the covariance function in (29),

$$\int_0^t C_\kappa(x,x-b)\,\mathrm{e}^{mb\mathrm{Da}}\mathrm{d}b = 2\sum_{i=1}^N \phi_i(x)\int_0^t \phi_i(x-b)\,\mathrm{e}^{mb\mathrm{Da}}\mathrm{d}b, \tag{57}$$

where $m = 2$ or $m = 1$ in (47) or (48), respectively. For the bases functions $\phi_i(x)$ in (30), the integral on the right-hand-side becomes

$$\int_0^t \phi_k(z)\mathrm{e}^{mb\mathrm{Da}}\mathrm{d}b = \Phi(b=t,z) - \Phi(b=0,z), \tag{58}$$

where

$$\Phi(b,z) \stackrel{\text{def}}{=} \frac{\mathrm{Da}L^2 m\,\mathrm{e}^{mb\mathrm{Da}}}{2\lambda^k(4k^2+\mathrm{Da}^2L^2m^2)}\left[1-\cos\left(\frac{2kz}{L}\right)+\frac{4k^2}{\mathrm{Da}^2L^2m^2}+\frac{2k}{\mathrm{Da}Lm}\sin\left(\frac{2kz}{L}\right)\right]. \tag{59}$$

Substituting (57)–(59) into (47) and (48) yields closed-form analytical expressions for D_{44} and U_4, respectively. Accounting for (23), the mean reaction rate in (48) is

$$\langle\kappa(x;\omega)\rangle = \sum_{j=1}^{N}\phi_j(x). \tag{60}$$

In contrast to their counterparts in [1], our expressions for the mean reaction rate, the diffusion coefficient D_{44} and the effective velocity U_4 vary in x. This is due to the fact that the covariance function $C_\kappa(x,y)$ we have considered is *not homogeneous*.

3.3.2. Coefficients for the uniform reaction rate model

Substituting (35) into (47) and (48) yields

$$D_{44}(a,t) = \frac{\sigma_\kappa^2\mathrm{Da}^2(a-1)^2}{2(2\mathrm{Da}\ell-1)}\begin{cases}\mathrm{e}^{(2\mathrm{Da}\ell-1)t/\ell}-1 & t\leqslant T(a)\\ \mathrm{e}^{(2\mathrm{Da}\ell-1)T/\ell}-1 & t>T(a)\end{cases} \tag{61}$$

and

$$U_4(a,t) = \mathrm{Da}(1-a)K - \frac{\sigma_\kappa^2\mathrm{Da}^2(a-1)}{2(\mathrm{Da}\ell-1)}\begin{cases}\mathrm{e}^{(\mathrm{Da}\ell-1)t/\ell}-1 & t\leqslant T(a)\\ \mathrm{e}^{(\mathrm{Da}\ell-1)T/\ell}-1 & t>T(a)\end{cases} \tag{62}$$

where $T(a)$ is defined in (49). The following limiting values are of interest,

$$D_{44}(0,t)=0,\quad D_{44}(1,t)=0,\quad U_4(0,t)=K\mathrm{Da},\quad U_4(1,t)=0. \tag{63}$$

Fig. 8 exhibits the dispersion coefficient D_{44} and effective velocity U_4 for different ℓ.

As the correlation length increases ($\ell\to\infty$), $D_{44}\to 0$ and $u_4\to\mathrm{Da}(1-a)K$. In this regime, the LED-based PDF equation (46) reduces to a first-order advection equation

$$\frac{\partial p^{(a)}_{c(x,t)}}{\partial t} = -\frac{\partial p^{(a)}_{c(x,t)}}{\partial x} - \mathrm{Da}K\frac{\partial\left[(1-a)p^{(a)}_{c(x,t)}\right]}{\partial a}. \tag{64}$$

This equation can also be derived directly from (21) by noting that in the limit of $\ell\to\infty$ the random reaction rate (34) becomes deterministic and equal to K. Then applying the PDF methods described in Section 2.1 directly to (21) leads to (64) without any closure approximation. This provides a demonstration of self-consistency and exactness of the LED-based closure, at least in the limit of $\ell\to\infty$.

3.3.3. Coefficients for the uncorrelated reaction rate model

The exponential covariance (35) is an element of a delta sequence, i.e. it converges to $\sigma_\kappa^2\delta(x-y)$ as $\ell\to 0$. This suggests that the coefficients for a delta-correlated random reaction rate $\kappa(x;\omega)$ can be obtained by taking the limit of (61), (62) as $\ell\to 0$. Since

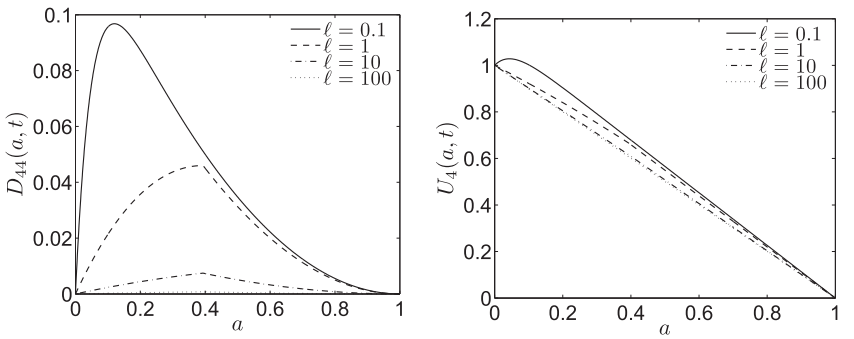

Fig. 8. Effective diffusivity (61) and effective velocity (62) for the exponentially correlated random reaction model. Shown are results at $t=1$ for different correlation lengths and $\mathrm{Da}=0.5, \sigma_\kappa=1, K=2$.

$$\lim_{\ell\to 0}\frac{e^{(J\ell-1)R/\ell}-1}{(J\ell-1)}=1 \quad \forall R\neq 0 \text{ and } \forall J\neq 1/\ell, \tag{65}$$

this limit yields (for $a\neq 0$)

$$C_\kappa(x,y)=\sigma_\kappa^2\delta(x-y), \quad D_{44}(a)=\frac{\mathrm{Da}^2\sigma_\kappa^2}{2}(1-a)^2, \quad U_4(a)=\mathrm{Da}\left(K+\frac{\mathrm{Da}\sigma_\kappa^2}{2}\right)(1-a). \tag{66}$$

It has been shown in [1] that with these coefficients the LED approximation coincides exactly with Fokker–Planck equation of the system (see also [24]). Note that if $R\to 0$ in (65), i.e. if $a\to 0$ (see Eqs. (61)), then the limit has to modified. A straightforward analysis indeed shows that $D_{44}(0)=0$ and $U_4(0)=\mathrm{Da}K$. The plots of D_{44} and $U_4(0)=\mathrm{Da}K$ for very small ℓ are shown in Fig. 9.

3.4. Analytical solutions for the PDF of the concentration field

In addition to solving the PDF equations introduced above, we derive a single-point PDF of the state variable $c(x,t;\omega)$ by solving the initial-boundary value problem (21), (22) and then using this solution to relate its PDF to the joint PDF of the input parameters.

3.4.1. Chi-squared reaction rate model

We show in appendix B that a solution of (21), (22) with the reaction rate $\kappa(x;\omega)$ parametrized by (23) has the form

$$c(x,t;\omega)=1-\begin{cases}\mathrm{e}^{-\mathrm{Da}Q(x,t;\omega)} & x\geqslant t\\ \mathrm{e}^{-\mathrm{Da}Q(x,x;\omega)} & x\leqslant t\end{cases}, \quad Q(x,t;\omega)\overset{\text{def}}{=}\sum_{k=1}^{N}\chi_k(\omega)h_k(x,t) \tag{67}$$

where

$$h_k(x,t)\overset{\text{def}}{=}\frac{t}{2\lambda^k}-\frac{\sin(2kx/L)-\sin[2k(x-t)/L]}{4k\lambda^k/L}. \tag{68}$$

One can show that $Q(x,t;\omega)\geqslant 0$ for all (x,t), so that the random concentration $c(x,t;\omega)\in[0,1]$ with probability one. The exponents of the product $\chi_k(\omega)t$ in the analytical solution (67) suggests that a direct numerical simulation of the initial-boundary value problem (21), (22) using polynomial chaos or probabilistic collocation is likely to loose accuracy in time. This is known to yield a long-term integration problem for polynomial chaos methods [14,15]. Since $Q(x,t;\omega)$ is a linear combination of chi-squared random variables, its PDF is

$$p^{(a)}_{Q(x,t)}=\frac{1}{\beta}\sum_{j=0}^{\infty}d_j(x)q_{N+2j}\left(\frac{a}{\beta}\right), \tag{69}$$

where β is an arbitrary positive parameter, $q_{N+2j}(a/\beta)$ is given by (27), and $d_j(x)$ satisfy the recurrence relation (27) with $\phi_i(x)$ replaced by $h_i(x,t)$. Thus, the *exact* one-point PDF of $c(x,t;\omega)$ is given by ([56, p. 93])

$$p^{(a)}_{c(x,t)}=\frac{1}{\mathrm{Da}(1-a)}\begin{cases}p^{(-\ln(1-a)/\mathrm{Da})}_{Q(x,t)} & x\geqslant t\\ p^{(-\ln(1-a)/\mathrm{Da})}_{Q(x,x)} & x\leqslant t\end{cases} \qquad a\in[0,1]. \tag{70}$$

This solution is analogous to the PDF solution given by Eqs. (12)–(23) in [24], which treated the random reactive rate exactly, without resorting to the expansion (23). Fig. 10 exhibits several time snapshots of the single-point PDF in (70) for $\mathrm{Da}=1$ and $\lambda=1.5$.

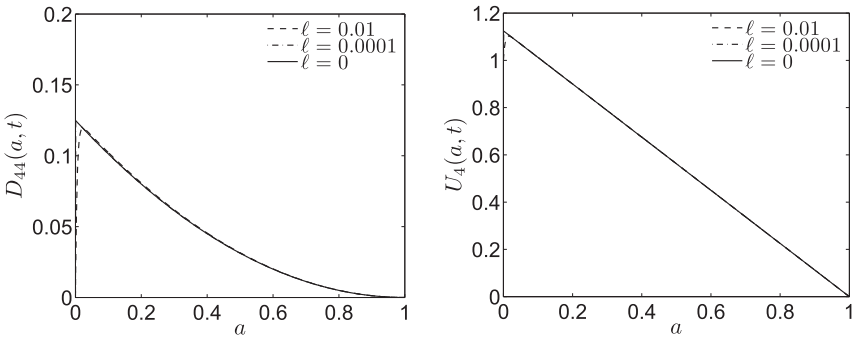

Fig. 9. Effective diffusivity (61) and effective velocity (62) for the exponentially correlated random reaction model. Shown are results at $t=1$ for $\mathrm{Da}=0.5, \sigma_\kappa=1, K=2$ and very small correlation lengths.

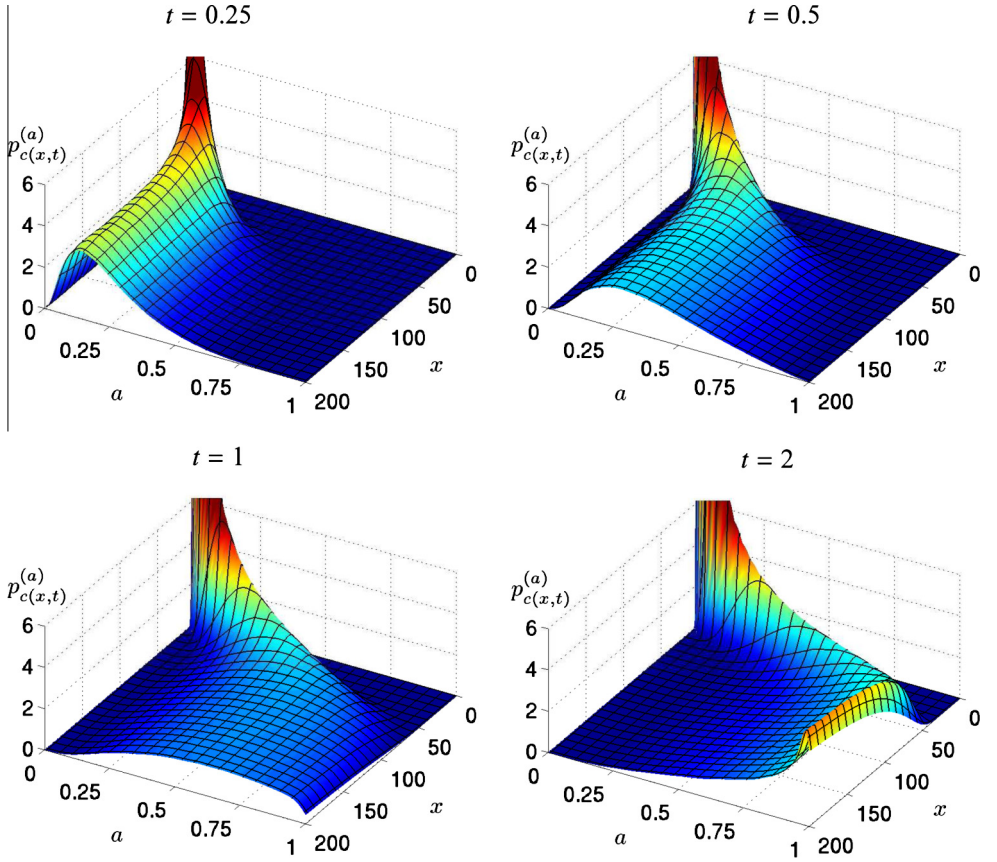

Fig. 10. Time-snapshots of the exact one-point PDF of the random concentration field (70) arising in linear reactions ($\alpha = 1$) for Damköhler number $\mathrm{Da} = 1$ and the chi-squared distributed random reaction rate $\kappa(x;\omega)$ with $\lambda = 1.5$ (see §3.1).

3.4.2. Uniform reaction rate model

We show in appendix B that a solution of (21), (22) with the reaction rate $\kappa(x;\omega)$ parametrized by (34) has the form

$$c(x,t;\omega) = 1 - \begin{cases} e^{-\mathrm{DaQ}(x,t;\omega)} & x \geqslant t \\ e^{-\mathrm{DaQ}(x,x;\omega)} & x \leqslant t \end{cases}, \quad Q(x,t;\omega) \stackrel{\text{def}}{=} Kt + \frac{\sqrt{3}\sigma_\kappa}{\sqrt{2\ell}} \sum_{k=1}^{N} \zeta_k(\omega) d_k(x,t) \tag{71}$$

where

$$d_k(x,t) \stackrel{\text{def}}{=} \frac{\ell\sqrt{\theta_k}}{A_k}\left(\sin(z_k x) - \sin[z_k(x-t)] - \frac{\cos(z_k x) - \cos[z_k(x-t)]}{\ell z_k}\right). \tag{72}$$

The procedure followed in the previous section to obtain the exact one-point PDF of the concentration field can be repeated for uniform random reaction rates. However, as we have anticipated in Section 3.1.2, the exact formula for the PDF of a superimposition of uniform independent random variables is rather involved (e.g., [55,54]). Instead, we consider a non-parametric estimate of the concentration PDF based on the analytical solution (71). Fig. 11 exhibits four time snapshots of the resulting PDF at $x = 25$ for $\sigma_\kappa\sqrt{3}/\sqrt{2\ell} = 0.25, K = 0.75$ and different correlation lengths. The cases $\ell = 300, \ell = 50$ and $\ell = 1$ are rather similar to each others. However, the *random paths* of the solution field $c(x,t;\omega)$ are completely different for different ℓ, as shown in Fig. 12.

According to the central limit theorem, for $\ell \to 0$ the exponent in (71) is Gaussian for each fixed x and t (summation of many independent random variables). In addition, the variance $\mathrm{Var}(x,t) \stackrel{\text{def}}{=} (1/3)\sum_{i=1}^{N} d_i(x,t)^2$ of the series

$$\sum_{i=1}^{N} \zeta_i(\omega) d_i(x,t) \tag{73}$$

has a limit for $\ell \to 0$ which does not depend on x (see Fig. 13). Such limit value is identified as

$$\mathrm{Var}(x,t) \stackrel{\ell \to 0}{\to} 2\ell t/3. \tag{74}$$

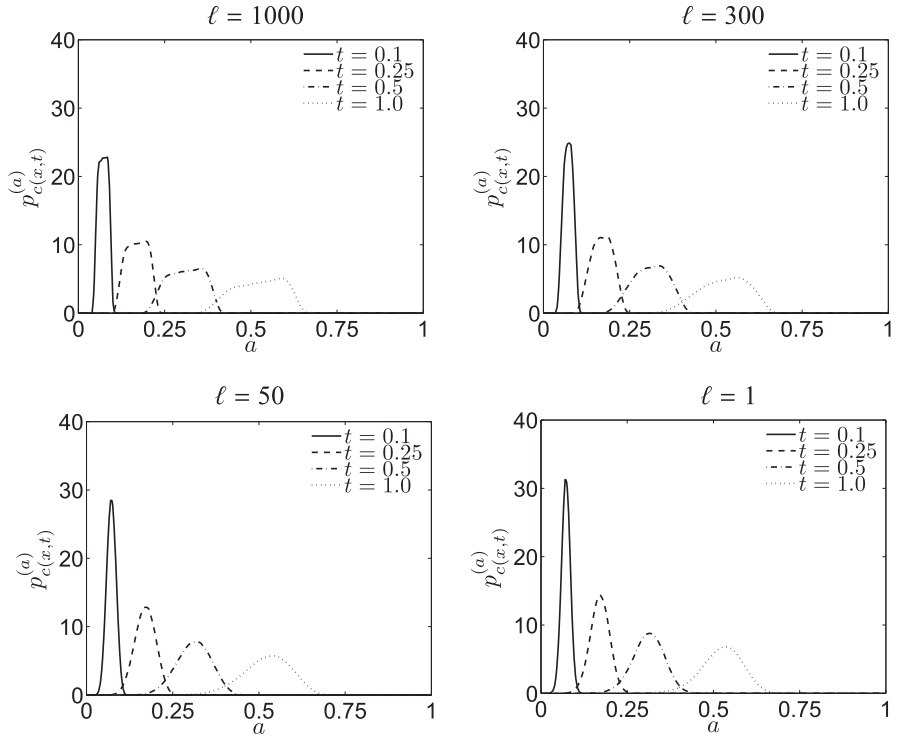

Fig. 11. Time snapshots of the one-point PDF of the random concentration field at $x = 25$ for $\sigma_\kappa\sqrt{3}/\sqrt{2\ell} = 0.25$ and $K = 0.75$. Shown are results obtained with different correlation lengths and $\mathrm{Da} = 1$.

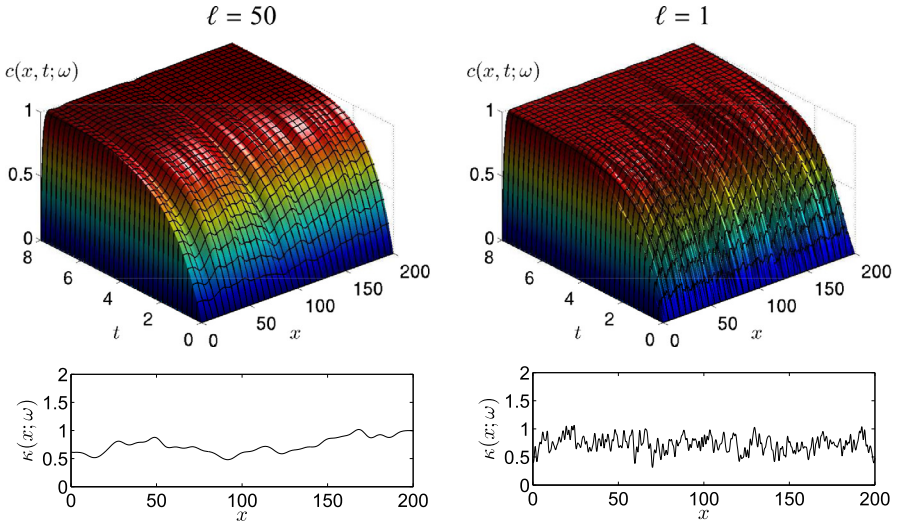

Fig. 12. Realizations of the random concentration field (71) (first row) corresponding to the realizations of random reaction rate shown in the second row. The reaction rate samples are obtained for $\sigma_\kappa\sqrt{3}/\sqrt{2\ell} = 0.25, K = 0.75$ and correlation lengths $\ell = 50$ (left) and $\ell = 1$ (right). The Damköhler number is set to $\mathrm{Da} = 1$.

This implies that for small correlation lengths, i.e., for Gaussian white-noise random reaction rates, the PDF of the concentration field is Gaussian and explicitly given by

$$p^{(a)}_{c(x,t)} = \frac{1}{\sqrt{2\pi}\mathrm{Da}(1-a)\sigma_\kappa}\begin{cases} S(t) & x \geqslant t \\ S(x) & x \leqslant t \end{cases}, \quad S(z) \overset{\text{def}}{=} \frac{1}{\sqrt{z}}\exp\left[-\frac{(\ln(1-a)/\mathrm{Da} + Kz)^2}{2\sigma_\kappa^2 z}\right]. \tag{75}$$

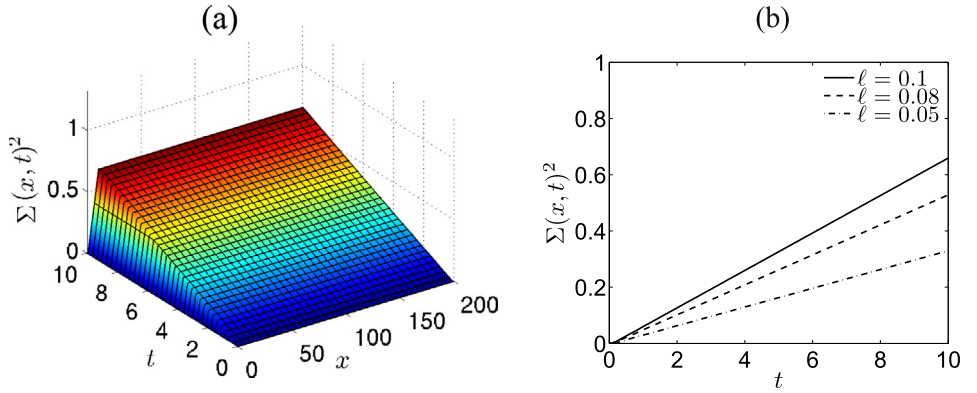

Fig. 13. (a) Contour plot of $\mathrm{Var}(x,t)$ for $\ell = 0.1$. (b) Time evolution of $\mathrm{Var}(x,t)$ at $x = 100$ for different correlation lengths ℓ. Figure (b) shows that $\mathrm{Var}(x,t) = 2\ell t/3$ for $\ell \to 0$ and $x \geqslant t$, regardless on the value of x (left).

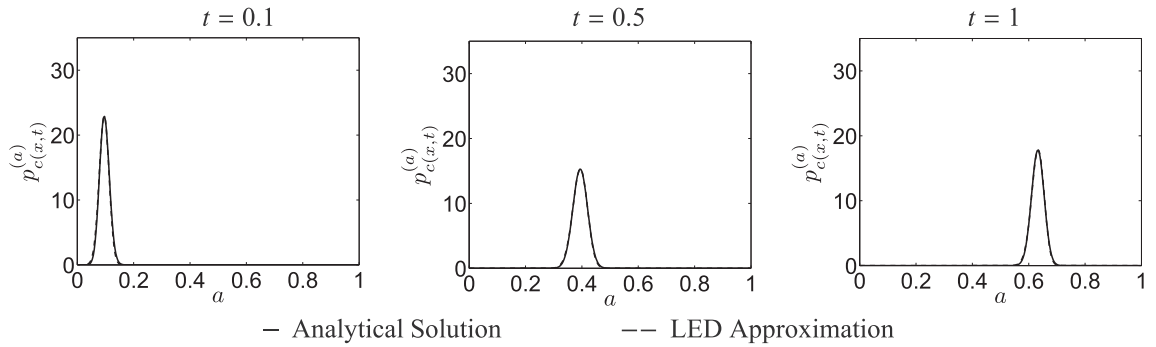

Fig. 14. Time-snapshots of the PDF of the random concentration field at $x = 50$ for uncorrelated (Gaussian white-noise type) random reaction rates. Shown is the comparison between the numerical solution to (52) and the analytical result (75) for $K = 2, \mathrm{Da} = 0.5$ and $\sigma_\kappa = 0.12$.

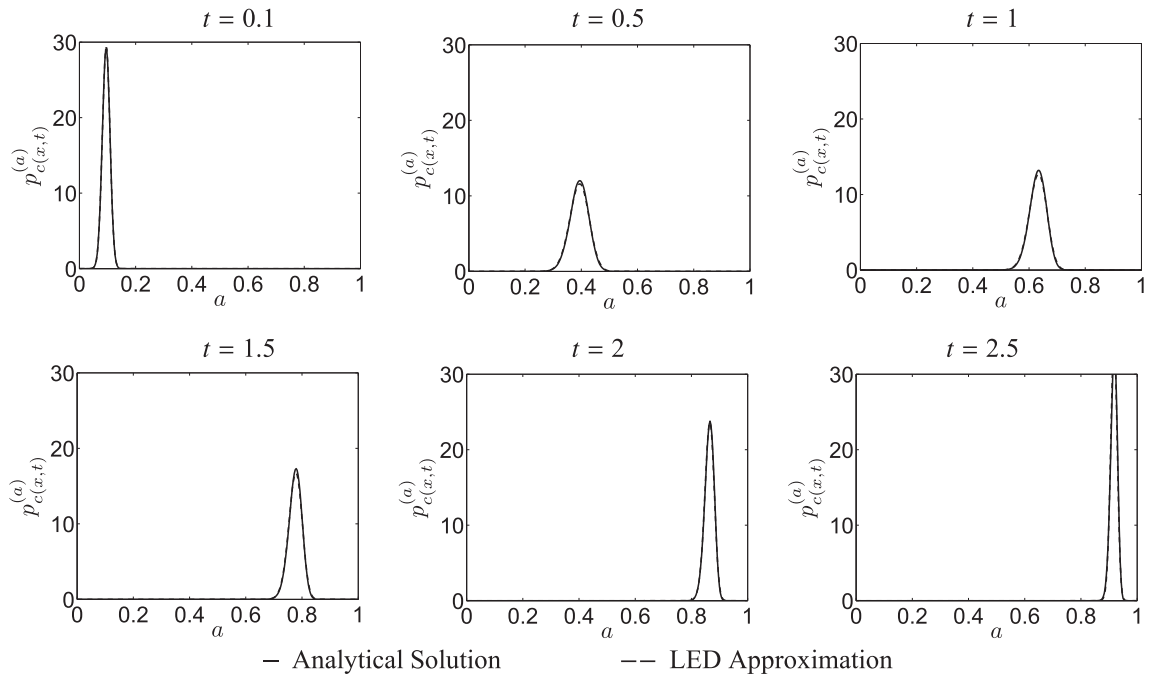

Fig. 15. Time-snapshots of the PDF of the random concentration field at $x = 100$ for weakly correlated ($\ell = 0.1$) random reaction rates. Shown is the comparison between the numerical solution to Eq. (52) and the PDF obtained from the analytical solution (71). We have set $K = 2, \mathrm{Da} = 0.5, \ell = 0.1$ and $\sigma_\kappa = K\sqrt{2\ell}/(3\sqrt{3})$ in order for the random reaction rate to be positive with probability one. With these parameters, the standard deviation of the random reaction rate is about 33% of the mean value K (see (34)).

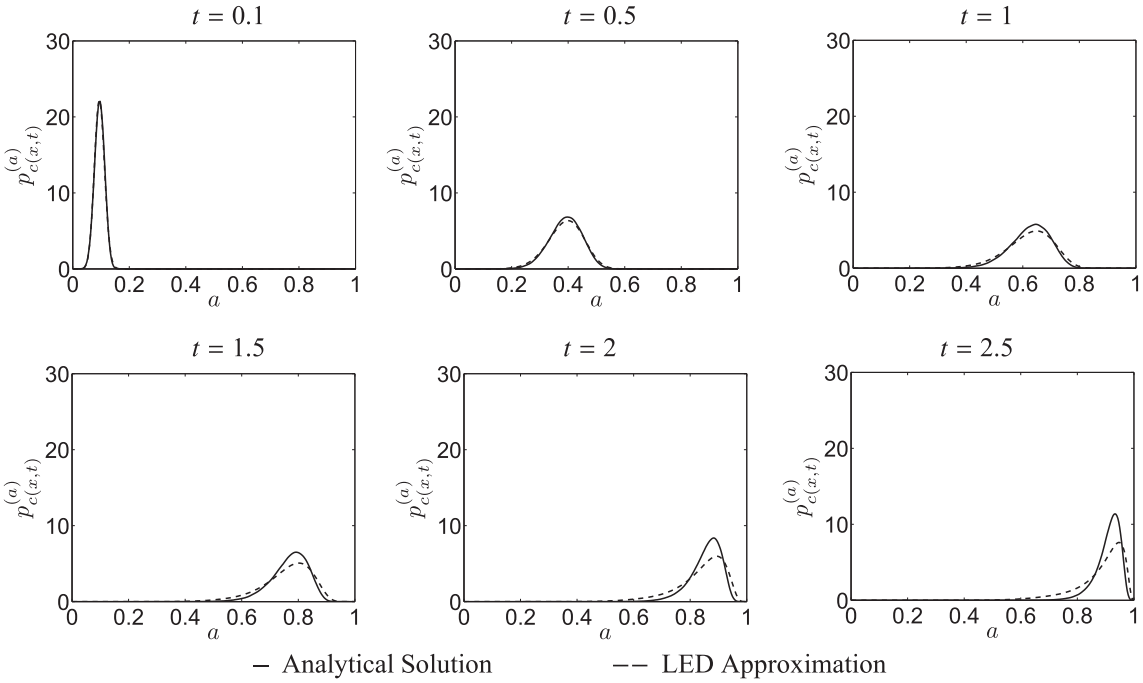

Fig. 16. Same as Fig. 15 but with $\ell = 10$.

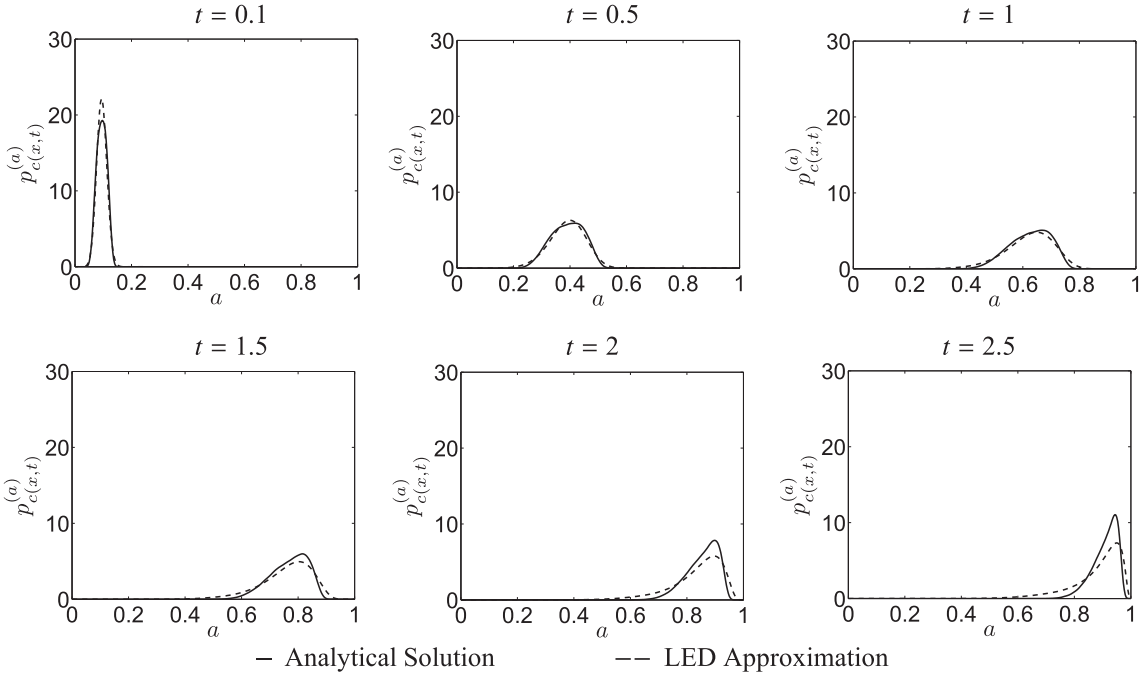

Fig. 17. Same as Fig. 15 but with $\ell = 100$.

4. Numerical results

In order to solve the initial/boundary value problem (52)–(56) we employed a conditionally stable time integration scheme for advection–diffusion equations. Specifically, we discretized (52) by using a second-order central finite difference scheme with an explicit third-order Runge–Kutta time stepping. A numerical solution to (52) was then used to compute the one-point PDF by numerically differentiating $\mathcal{P}^{(a)}_{c(x,t)}$ with respect to a, since

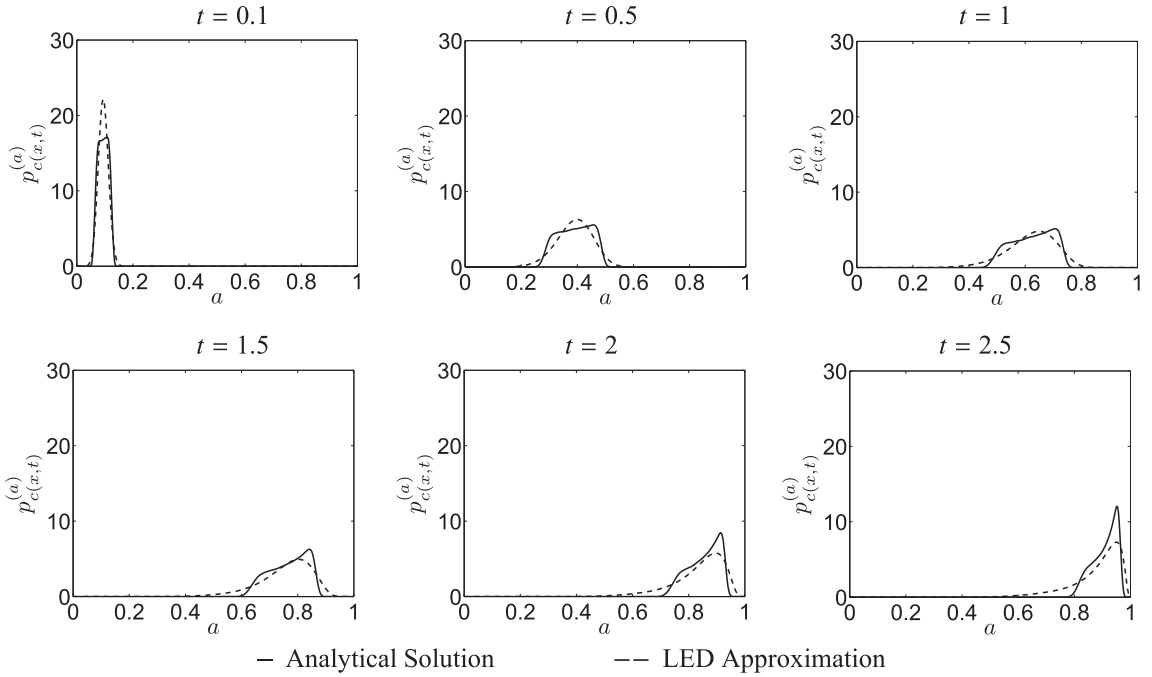

Fig. 18. Same as Fig. 15 but with $\ell = 1000$.

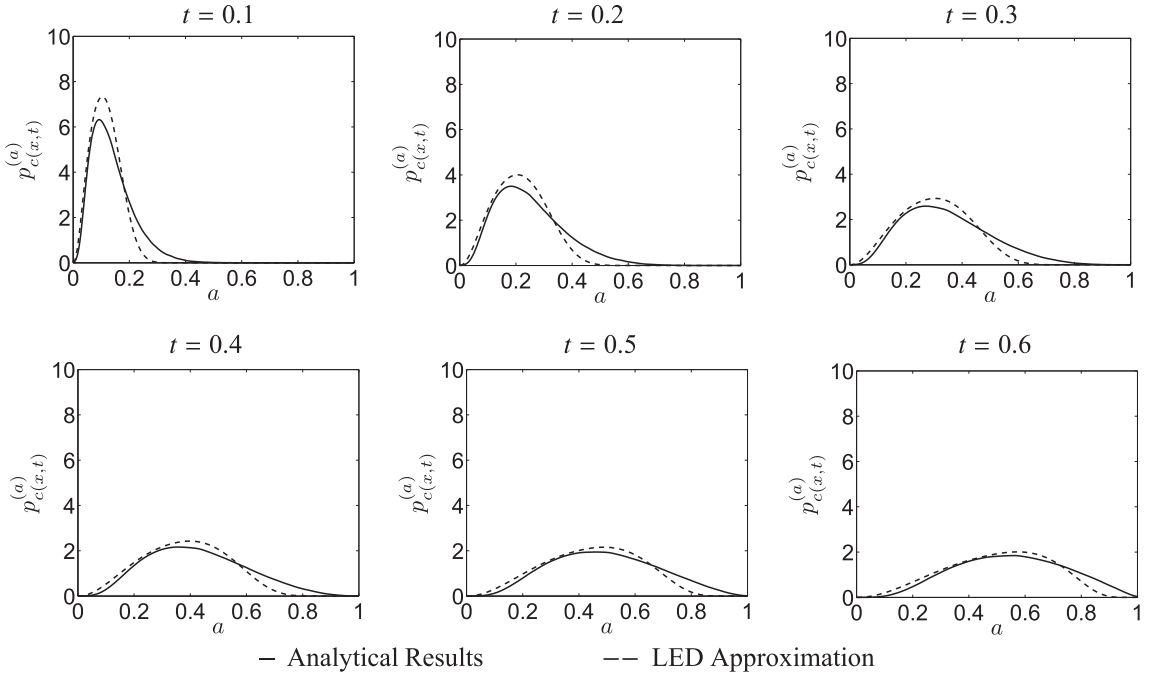

Fig. 19. Comparison between the one-point one-time PDF as obtained from the exact analytical formula (70) (continuous line) and the LED approximation (52) (dashed line). Shown are different time snapshots at location $x = 100$. The Damköhler number is set at $\mathrm{Da} = 1$, while the parameters used for the random reaction rate (23) are $N = 20$ and $\lambda = 1.5$ (see Eq. (30)).

$$p^{(a)}_{c(x,t)} = \frac{\partial \mathcal{P}^{(a)}_{c(x,t)}}{\partial a}. \tag{76}$$

The latter step may reduce the overall accuracy of the PDF representation.

4.1. Uncorrelated reaction rate model

For uncorrelated random reaction rates the LED closure is exact. Therefore, the numerical solution to (52) whose coefficients are given by (66) should match exactly the analytical PDF in (75). Fig. 14 demonstrates this to be the case. A fundamental question is whether the LED approximation produces reliable results also for weakly or strongly correlated random reaction rates.

4.2. Uniform reaction rate model

Figs. 15–18 exhibit time snapshots of the one-point PDF of the random concentration field corresponding to random reaction rates with increasing correlation lengths. As the correlation length of the random reaction rate increases the LED approximation becomes less accurate, while continuing to maintain a good qualitative statistical description. Note that in all cases, the LED approximation leads to PDFs whose tails are fatter than those of their exact counterparts. In other words, the LED-based PDF equations provide a *conservative estimate* of the predictive uncertainty.

As demonstrated in Section 3.3.2, the LED approximation is exact for very large ℓ. However, our positivity constraint on $\kappa(x;\omega)$ imposes $\sigma_\kappa = K\sqrt{2\ell}/(w(\ell)\sqrt{3})$, with $w(\ell)$ depending on ℓ and bounded from below (see Fig. 5). This means that, if we set $w(\ell) = 3$ as we have done here we have, for $\ell \to \infty$,

$$k(x;\omega) \to K[1 + \vartheta\zeta_1(\omega)], \quad \vartheta \in \mathbb{R}^+, \quad \zeta_1(\omega) \text{ uniform in } [-1,1]. \tag{77}$$

Therefore, we never reach the conditions for which the LED approximation is exact. This justifies the deviation between the analytical solution and the numerical solution to the LED-based PDF equation observed in Fig. 18.

4.3. Chi-squared reaction rate model

For the reaction rate with the *inhomogeneous* correlation function introduced in Section 3.1, the diffusion coefficient D_{44} and effective velocity u_4 in (52) are given by (47)–(59). Fig. 19 shows the time snapshots of the one-point PDF computed with both the LED closure (52) and the exact analytical solution (70), at $x = 100$ for $\lambda = 1.5$. The LED closure introduces some errors into the PDF dynamics. This is to be expected from the results reported in the previous section. The LED closure is exact for white-noise Gaussian random processes, and its accuracy decreases as the correlation length increases. Despite the minor accuracy problem, the overall advantages of the LED closure approximation are evident. In particular, the dimensionality of the LED approximation is much lower than that of the exact joint PDF equation. This eventually allows for an effective simulation of high-dimensional advection–reaction systems.

5. Summary

We investigated two general frameworks for computing the probability density function (PDFs) of radom scalar fields whose dynamics is governed by advection–reaction equations (AREs) with uncertain advection velocity and reaction rates. These approaches are the single-point PDF equation based on a large-eddy diffusivity (LED) closure approximation [1], and the joint PDF equation based on decomposition of random system parameters into finite series of random variables. We compared the solutions of these two equations with analytical solutions to an ARE, whose linear reaction law was parametrized by random reaction rates defined in terms of either chi-squared or uniform random variables. This allowed us to test the accuracy of the LED-based PDF equation on a reliable basis. We found that the LED closure is exact both for white-noise Gaussian random reaction rates and for reaction rates having an infinite correlation length. For intermediate correlation lengths, the accuracy of the LED closure decreases, while continuing to maintain a good qualitative statistical description. In all cases, the LED approximation leads to PDFs, whose tails are fatter than those of their exact counterparts. In other words, the LED-based PDF equations provide a conservative estimate of the predictive uncertainty.

The computational advantages of the closure approximation are evident for input uncertainties characterized in terms of a large number of random variables. Indeed, the exact PDF (or CDF) equation of the system in these cases is high-dimensional and therefore its solution requires appropriate numerical techniques such as sparse grid [57,31,7] or functional ANOVA [58,32,33]. More generally, for stochastic PDEs of order greater than one closures are unavoidable since an exact exact equation for the one-point one-time PDF does not exist due to the non-locality (in space and time) of the solution. In these cases, the closure may be based, e.g., on a truncation of the exact Hopf functional equation leading to a hierarchy of equations for the cumulants of the solution [59,18,17] or to a truncated Lundgren-Monin-Novikov hierarchy [21]. Alternatively other closures such as direct interaction approximations [43,60], conditional closures [61,62] and mapping closures [63,64] (see also [65]) can be considered.

Acknowledgments

We acknowledge financial support from DOE (Grant No. DE-FG02-07ER25818), OSD-MURI (Grant No. FA9550-09-1-0613) and NSF (Grant No. DMS-0915077).

Appendix A. Analytical solution to the exact joint PDF equation

We solve the initial-boundary value problem (40)–(45) by using the method of characteristics [47]. The (random) characteristics curves of the system, $\hat{t}(s,t,x,a), \hat{x}(s,t,x,a), \hat{a}(s,t,x,a)$ and $\hat{z}(s,t,x;\boldsymbol{b})$, satisfy the equations

$$\frac{\partial \hat{t}}{\partial s}=1, \quad \frac{\partial \hat{x}}{\partial s}=1, \quad \frac{\partial \hat{a}}{\partial s}=\mathrm{Da}H(\hat{x})(1-\hat{a}), \quad \frac{\partial \hat{z}}{\partial s}= \mathit{Da}H(\hat{x})\hat{z}, \quad H(x)\stackrel{\mathrm{def}}{=}\sum_{i=1}^{N}\phi_i(x)b_i, \tag{A.1}$$

subject to one of the three sets of auxiliary conditions

$$\hat{t}(0,t,x,a)=0, \quad \hat{x}(0,t,x,a)=x, \quad \hat{a}(0,t,x,a)=a, \quad \hat{z}(0,t,x,a)=\delta(a)p_{\boldsymbol{\chi}}^{(\boldsymbol{b})}; \tag{A.2}$$

$$\hat{t}(0,t,x,a)=t, \quad \hat{x}(0,t,x,a)=0, \quad \hat{a}(0,t,x,a)=a, \quad \hat{z}(0,t,x,a)=\delta(a)p_{\boldsymbol{\chi}}^{(\boldsymbol{b})}; \tag{A.3}$$

or

$$\hat{t}(0,t,x,a)=t, \quad \hat{x}(0,t,x,a)=x, \quad \hat{a}(0,t,x,a)=0, \quad \hat{z}(0,t,x,a)=0; \tag{A.4}$$

depending on whether the characteristics originate at the $(a,x,0),(a,0,t)$, or $(0,x,t)$ plane, respectively.

Let us consider the set of characteristic curves departing from the $(a,x,0)$ plane (the analogous procedure is to be performed for the other two cases). Integration of the system (A.1) with the initial conditions (A.2) yields

$$\hat{t}=s, \quad \hat{x}=s+x, \quad \int_{\hat{a}(0)}^{\hat{a}}\frac{\mathrm{d}b}{1-b}=\mathrm{Da}\mathcal{I}(s,x,\boldsymbol{b}), \quad \int_{\hat{z}(0)}^{\hat{z}}\frac{\mathrm{d}b}{b}=\mathrm{Da}\mathcal{I}(s,x,\boldsymbol{b}). \tag{A.5}$$

where

$$\mathcal{I}(s,x,\boldsymbol{b})\stackrel{\mathrm{def}}{=}\int_0^s H(x+s)ds=\sum_{k=1}^{N}\frac{b_k(\omega)}{\lambda^k}\left(\frac{s}{2}-\frac{\sin(2k(x+s)/L)-\sin(2kx/L)}{4k/L}\right). \tag{A.6}$$

Integrating the last equation in (A.5) we obtain

$$\hat{z}=\delta(a)\,p_{\boldsymbol{\chi}}^{(\boldsymbol{b})}\,\mathrm{e}^{\mathrm{Da}\,\mathcal{I}(s,x,\boldsymbol{b})}. \tag{A.7}$$

Solving the third equation in (A.5) for $a=\hat{a}(0)$, and substituting the result into (A.7), gives

$$p_{c(x,t)\boldsymbol{\chi}}^{(a,\boldsymbol{b})}=\delta\left[a+\mathrm{e}^{-\mathrm{Da}\mathcal{I}(t,x-t,\boldsymbol{b})}\right]p_{\boldsymbol{\chi}}^{(\boldsymbol{b})}\mathrm{e}^{\mathrm{Da}\mathcal{I}(t,x-t,\boldsymbol{b})}. \tag{A.8}$$

Note that this representation involves a nonlinear transformation inside the delta function, which needs to be properly handled [42].

Repeating these mathematical steps for the characteristic curves arising from the other two planes, $(a,0,t)$ and $(0,x,t)$, we obtain the analytical expression for the joint PDF $p_{c(x,t)\boldsymbol{\chi}}^{(a,\boldsymbol{b})}$ that is valid over its domain of definition. The regions of the space (a,x,t) where each of the three families of characteristics holds is determined by studying the characteristic curves arising from the intersections of the planes $(a,x,0),(a,0,t)$ and $(0,x,t)$, namely, the lines $(a,0,0),(0,x,0)$ and $(0,0,t)$. Finally, an integration of the analytical expression for $p_{c(x,t)\boldsymbol{\chi}}^{(a,\boldsymbol{b})}$ with respect to $b_1,\ldots,b_N$ yields the one-point PDF of the concentration field (70).

Appendix B. Analytical solution to the advection–reaction problem in physical space

We solve the initial-boundary value problem (21), (22) by using the method of characteristics [47]. The (random) characteristic curves of the system, $\hat{t}(s,t,x),\hat{x}(s,t,x),\hat{z}(s,t,x;\omega)$, satisfy the equations

$$\frac{\partial \hat{t}}{\partial s}=1, \quad \frac{\partial \hat{x}}{\partial s}=1, \quad \frac{\partial \hat{z}}{\partial s}=(1-\hat{z})\kappa(\hat{x};\omega)\mathrm{Da}, \tag{B.1}$$

subject to the initial conditions

$$\hat{t}(0,t,x)=0, \quad \hat{x}(0,t,x)=x, \quad \hat{z}(0,t,x;\omega)=0, \tag{B.2}$$

or

$$\hat{t}(0,t,x)=t, \quad \hat{x}(0,t,x)=0, \quad \hat{z}(0,t,x;\omega)=0, \tag{B.3}$$

depending on where the characteristic comes from, i.e., from the $(x,0)$ axis or the $(0,t)$ axis, respectively. Let us first consider the characteristics arising from the $(x,0)$ axis. By integrating (B.1) with initial conditions (B.2) we obtain

$$\hat{t}=s, \quad \hat{x}=x+s, \quad \int_0^{\hat{z}(s)}\frac{\mathrm{d}b}{1-b}=\mathrm{Da}\int_0^s\kappa(x+\tau)\mathrm{d}\tau. \tag{B.4}$$

Depending on the specific choice of the random reaction rate $\kappa(x;\omega)$ (see section 3.1.1 and Section 3.1.2) the integral appearing in the last equation in (B.4) produces different expressions. For example, by using the representation (23) with ϕ_k given in (30), we obtain

$$\hat{z}(s,x;\omega) = 1 - \exp\left[-\mathrm{Da}\sum_{k=1}^{N}\frac{\chi_k(\omega)}{\lambda^k}\left(\frac{s}{2} - \frac{\sin(2k(x+s)/L) - \sin(2kx/L)}{4k/L}\right)\right]. \tag{B.5}$$

Similarly, along the characteristics curves arising from the $(0,t)$ axis (i.e., $\hat{t} = t + s$ and $\hat{x} = s$) we obtain

$$\hat{z}(s,x;\omega) = 1 - \exp\left[-\mathrm{Da}\sum_{k=1}^{N}\frac{\chi_k(\omega)}{\lambda^k}\left(\frac{s}{2} - \frac{\sin(2ks/L)}{4k/L}\right)\right]. \tag{B.6}$$

Expressing x and s in terms of the corresponding values $\hat{t}$ and $\hat{x}$ along the two groups of characteristics gives the analytical solution (67). Repeating these mathematical steps for the reaction rate model (34) gives the analytical solution (71).

References

[1] D.M. Tartakovsky, S. Broyda, PDF equations for advective-reactive transport in heterogeneous porous media with uncertain properties, J. Contam. Hydrol. 120–121 (2011) 129–140.
[2] D.M. Tartakovsky, C.L. Winter, Uncertain future of hydrogeology, ASCE J. Hydrol. Eng. 13 (1) (2008) 37–39.
[3] R.G. Ghanem, P.D. Spanos, Stochastic Finite Elements: A Spectral Approach, Springer-Verlag, 1998.
[4] D. Xiu, G.E. Karniadakis, The Wiener–Askey polynomial chaos for stochastic differential equations, SIAM J. Sci. Comput. 24 (2) (2002) 619–644.
[5] X. Wan, G.E. Karniadakis, Multi-element generalized polynomial chaos for arbitrary probability measures, SIAM J. Sci. Comput. 28 (3) (2006) 901–928.
[6] D. Venturi, X. Wan, G.E. Karniadakis, Stochastic bifurcation analysis of Rayleigh–Bénard convection, J. Fluid. Mech. 650 (2010) 391–413.
[7] J. Foo, G.E. Karniadakis, Multi-element probabilistic collocation method in high dimensions, J. Comput. Phys. 229 (2010) 1536–1557.
[8] X. Ma, N. Zabaras, An adaptive hierarchical sparse grid collocation method for the solution of stochastic differential equations, J. Comput. Phys. 228 (2009) 3084–3113.
[9] A. Nouy, Proper generalized decompositions and separated representations for the numerical solution of high dimensional stochastic problems, Arch. Comput. Meth. Appl. Mech. Eng. 17 (2010) 403–434.
[10] A. Nouy, O.P.L. Maître, Generalized spectral decomposition for stochastic nonlinear problems, J. Comput. Phys. 228 (2009) 202–235.
[11] D. Venturi, On proper orthogonal decomposition of randomly perturbed fields with applications to flow past a cylinder and natural convection over a horizontal plate, J. Fluid Mech. 559 (2006) 215–254.
[12] D. Venturi, X. Wan, G.E. Karniadakis, Stochastic low-dimensional modeling of a random laminar wake past a circular cylinder, J. Fluid Mech. 606 (2008) 339–367.
[13] D. Venturi, A fully symmetric nonlinear biorthogonal decomposition theory for random fields, Physica D 240 (4-5) (2010) 415–425.
[14] M. Gerritsma, J.-B. van der Steen, P. Vos, G. Karniadakis, Time-dependent generalized polynomial chaos, J. Comput. Phys. 229 (22) (2010) 8333–8363.
[15] X. Wan, G.E. Karniadakis, Long-term behavior of polynomial chaos in stochastic flow simulations, Comput. Meth. Appl. Mech. Eng. 195 (2006) 5582–5596.
[16] M.N. Özişik, Heat Conduction, second ed., John Wiley & Sons, 1993.
[17] A.S. Monin, A.M. Yaglom, Statistical fluid mechanics, Volume II: Mechanics of Turbulence, Dover, 2007.
[18] R.M. Lewis, R.H. Kraichnan, A space-time functional formalism for turbulence, Commun. Pure Appl. Math. 15 (1962) 397–411.
[19] G. Rosen, Dynamics of probability distributions over classical fields, Int. J. Theor. Phys. 4 (3) (1971) 189–195.
[20] D. Venturi, G.E. Karniadakis, Differential constraints for the probability density function of stochastic solutions to the wave equation, Int. J. Uncert. Quant. http://dx.doi.org/10.1615/Int.J.UncertaintyQuantification.2011003485.
[21] T.S. Lundgren, Distribution functions in the statistical theory of turbulence, Phys. Fluids 10 (5) (1967) 969–975.
[22] A.S. Monin, Equations for turbulent motion, Prikl. Mat. Mekh. 31 (6) (1967) 1057–1068.
[23] I. Hosokawa, Monin–Lundgren hierarchy versus the Hopf equation in the statistical theory of turbulence, Phys. Rev. E 73 (2006) 067301-1–067301-4.
[24] D.M. Tartakovsky, M. Dentz, P.C. Lichtner, Probability density functions for advective-reactive transport in porous media with uncertain reaction rates, Water Resour. Res. 45 (2009) W07414 (1–8).
[25] S. Broyda, M. Dentz, D.M. Tartakovsky, Probability density functions for advective-reactive transport in radial flow, Stoch. Environ. Res. Risk Assess. 24 (7) (2010) 985–992.
[26] D. Venturi, G.E. Karniadakis, New evolution equations for the joint response-excitation probability density function of stochastic solutions to first-order nonlinear pdes, J. Comput. Phys. Under Review.
[27] D. Venturi, T.P. Sapsis, H. Cho, G.E. Karniadakis, A computable evolution equation for the joint response-excitation probability density function of stochastic dynamical systems, Proc. R. Soc. A http://dx.doi.org/10.1098/rspa.2011.0186.
[28] F. Chinesta, A. Ammar, E. Cueto, Recent advances and new challenges in the use of the proper generalized decomposition for solving multidimensional models, Arch. Comput. Meth. Appl. Mech. Eng. 17 (4) (2010) 327–350.
[29] A. Nouy, A priori model reduction through proper generalized decomposition for solving time-dependent partial differential equations, Comput. Meth. Appl. Mech. Eng. 199 (2010) 1603–1626.
[30] G. Leonenko, T. Phillips, On the solution of the Fokker–Planck equation using a high-order reduced basis approximation, Comput. Meth. Appl. Mech. Eng. 199 (1–4) (2009) 158–168.
[31] E. Novak, K. Ritter, Simple cubature formulas with high polynomial exactness, Constructive Approximation 15 (1999) 499–522.
[32] Y. Cao, Z. Chen, M. Gunzburger, ANOVA expansions and efficient sampling methods for parameter dependent nonlinear PDEs, Int. J. Numer. Anal. Model. 6 (2009) 256–273.
[33] X. Yang, M. Choi, G.E. Karniadakis, Adaptive ANOVA decomposition of stochastic incompressible and compressible fluid flows, J. Comput. Phys. 231 (2012) 1587–1614.
[34] H. Rabitz, Ö.F. Aliş, J. Shorter, K. Shim, Efficient input–output model representations, Computer Phys. Commun. 117 (1–2) (1999) 11–20.
[35] D.M. Tartakovsky, A. Guadanini, F. Ballio, A.M. Tartakovsky, Localization of mean flow and apparent transmissivity tensor for bounded randomly heterogeneous aquifers, Transp. Porous Media 49 (1) (2002) 41–58.
[36] D.M. Tartakovsky, Z. Lu, A. Guadagnini, A.M. Tartakovsky, Unsaturated flow in heterogeneous soils with spatially distributed uncertain hydraulic parameters, J. Hydrol. 275 (2003) 182–193.
[37] K.D. Jarman, A.M. Tartakovsky, Divergence of solutions to solute transport moment equations, Geophys. Res. Lett. 35 (2008) L15401, http://dx.doi.org/10.1029/2008GL034495.
[38] K.D. Jarman, A.M. Tartakovsky, Divergence of solutions to perturbation-based advection-dispersion moment equations, Adv. Water Resour. 34 (2011) 659–670, http://dx.doi.org/10.1016/j.advwatres.2011.03.002.
[39] V.I. Klyatskin, Dynamics of Stochastic Systems, Elsevier Publishing Company, 2005.

[40] D.M. Tartakovsky, S.P. Neuman, Transient flow in bounded randomly heterogeneous domains 1. Exact conditional moment equations and recursive approximations, Water Resour. Res. 34 (1) (1998) 1–12.
[41] D.M. Tartakovsky, S.P. Neuman, Extension of Transient flow in bounded randomly heterogeneous domains. 1. Exact conditional moment equations and recursive approximations, Water Resour. Res. 35 (6) (1999) 1921–1925.
[42] R.P. Kanwal, Generalized functions: theory and technique, second ed., Birkhäuser Boston, 1998.
[43] R.H. Kraichnan, Lagrangian-history closure approximation for turbulence, Phys. Fluids 8 (4) (1965) 575–598.
[44] M. Dentz, D.M. Tartakovsky, Self-consistent four-point closure for transport in steady random flows, Phys. Rev. E 77 (6) (2008) 066307-1–066307-12.
[45] G. Dagan, Flow and Transport in Porous Formations, Springer-Verlag, New York, 1989.
[46] P. Wang, D.M. Tartakovsky, Uncertainty propagation in kinematic wave models, J. Comput. Phys. 231 (23) (2012) 7868–7880.
[47] H.-K. Rhee, R. Aris, N.R. Amundson, First-order partial differential equations, Volume 1: Theory and Applications of Single Equations, Dover, 2001.
[48] P.G. Moschopoulos, W.B. Canada, The distribution function of a linear combination of chi-squares, Comput. Math. Appl. 10 (4/5) (1984) 383–386.
[49] H. Ruben, Probability content of regions under spherical distributions, IV: the distribution of homogeneous and nonhomogeneous quadratic functions of normal variables, Ann. Math. Stat. 33 (1962) 542–570.
[50] S. Kotz, N.L. Johnson, D.W. Boyd, Series representations of distributions of quadratic forms in normal variables. I. central case., Ann. Math. Stat. 38 (1967) 823–837.
[51] H. Liu, Y. Tang, H.H. Zhang, A new chi-square approximation to the distribution of non-negative definite quadratic forms in non-central normal variables, Comput. Stat. Data Anal. 53 (2009) 853–856.
[52] R.H. Brown, The distribution function of positive definite quadratic forms in normal random variables, SIAM J. Sci. Comput. 7 (2) (1986) 689–695.
[53] M. Jardak, C.-H. Su, G.E. Karniadakis, Spectral polynomial chaos solutions of the stochastic advection equation, J. Sci. Comput. 17 (2002) 319–338.
[54] D.M. Bradley, R.C. Gupta, On the distribution of the sum of n non-identically distributed uniform random variables, Ann. Inst. Stat. Math. 54 (3) (2002) 689–700.
[55] M. Sadooghi-Alvandi, A.R. Nematollahi, R. Habibi, On the distribution of the sum of independent uniform random variables, Stat. Papers 50 (1) (2002) 171–175.
[56] A. Papoulis, Probability, Random Variables and Stochastic Processes, third ed., McGraw-Hill, 1991.
[57] M. Griebel, Sparse grids and related approximation schemes for higher dimensional problems, in: L.M. Pardo, A. Pinkus, E. Süli, M.J. Todd (Eds.), Foundations of Computational Mathematics, Santander 2005, 331, Cambridge University Press, 2006, pp. 106–161.
[58] G. Li, S.-W. Wang, H. Rabitz, S. Wang, P. Jaffé, Global uncertainty assessments by high dimensional model representations (HDMR), Chem. Eng. Sci. 57 (21) (2002) 4445–4460.
[59] U. Frisch, Turbulence: The Legacy of A.N. Kolmogorov, Cambridge University Press, 1995.
[60] H. Chen, S. Chen, R.H. Kraichnan, Probability distribution of a stochastically advected scalar field, Phys. Rev. Lett. 63 (1989) 2657–2660.
[61] M. Wilczek, A. Daitche, R. Friedrich, On the velocity distribution in homogeneous isotropic turbulence: correlations and deviations from Gaussianity, J. Fluid Mech. 676 (2011) 191–217.
[62] S.H. Kim, On the conditional variance and covariance equations for second-order conditional moment closure, Phys. Fluids 14 (6) (2002) 2011–2014.
[63] S.B. Pope, Mapping closures for turbulent mixing and reaction, Theor. Comput. Fluid Dyn. 2 (1991) 255–270.
[64] S.B. Pope, Pdf methods for turbulent reactive flows, Prog. Energy Combust. Sci. 11 (2) (1985) 119–192.
[65] S.B. Pope, Simple models of turbulent flows, Phys. Fluids 23 (2011) 011301-1–011301-20.